International Atomic Energy Agency

INDC(CCP)-217/LI

INDC INTERNATIONAL NUCLEAR DATA COMMITTEE

THE CONTRIBUTION OF DIRECT AND STATISTICAL REACTION MECHANISMS DURING FAST NEUTRON SCATTERING AT LOW-LYING LEVELS OF LIGHT AND MEDIUM NUCLEI

V.M. Bychkov, A.V. Ignatyuk and V.P. Lunev
Institute of Power Physics, Obninsk, USSR
D. Seeliger, S. Unholzer, D. Schmidt, T. Streil
and D. Hermsdorf
Technical University, Dresden, German Democratic Republic

Translated by the IAEA

December 1983

IAEA NUCLEAR DATA SECTION, WAGRAMERSTRASSE 5, A-1400 VIENNA

Reproduced by the IAEA in Austria
December 1983
84-00078

INDC(CCP)-217/LI

THE CONTRIBUTION OF DIRECT AND STATISTICAL REACTION MECHANISMS DURING FAST NEUTRON SCATTERING AT LOW-LYING LEVELS OF LIGHT AND MEDIUM NUCLEI

V.M. Bychkov, A.V. Ignatyuk and V.P. Lunev
Institute of Power Physics, Obninsk, USSR
D. Seeliger, S. Unholzer, D. Schmidt, T. Streil
and D. Hermsdorf
Technical University, Dresden, German Democratic Republic

Translated by the IAEA

December 1983

L83-23007
Translated from Russian

Fiz. Ehlem. Chastits At. Yadra 14, 2 (1983)

UDC.539.172

THE CONTRIBUTION OF DIRECT AND STATISTICAL REACTION MECHANISMS DURING FAST NEUTRON SCATTERING AT LOW-LYING LEVELS OF LIGHT AND MEDIUM NUCLEI

V.M. Bychkov, A.V. Ignatyuk and V.P. Lunev
Institute of Power Physics, Obninsk, USSR
D. Seeliger, S. Unholzer, D. Schmidt, T. Streil
and D. Hermsdorf
Technical University, Dresden, German Democratic Republic

ABSTRACT

The authors analyse the basic characteristics of the behaviour of the neutron excitation functions for low-lying levels of nuclei and discuss the interrelationship between these characteristics and the parameters of the optical and statistical models used for their description. They consider the differences in the parameters of the dynamic deformation of nuclei which occur in the direct inelastic nucleon scattering reactions and during Coulomb excitation of low-lying collective levels. It is shown that direct transitions make a substantial contribution to the excitation functions for discrete levels even at comparatively low neutron energies. The authors have investigated the role played by the structural changes of the neutron strength functions in the interpretation of the observed energy dependence of the inelastic scattering cross-sections in the near-threshold region.

INTRODUCTION

The study of the interaction of neutrons with atomic nuclei has been a subject of unflagging interest at all stages of development of nuclear physics. This is due, first of all, to the specific properties of the neutron, which unlike charged particles, can penetrate the nucleus and induce nuclear reactions at any arbitrarily small kinetic energy. For this reason, neutron absorption or scattering experiments are highly informative for the study of the resonance structure of nuclear reaction cross-sections and the associated properties of the excited states of nuclei. By increasing the incident neutron energy in such experiments we can make a detailed study of the whole range of effects occurring during the transition from isolated to overlapping resonances and, in the case of still higher energies, we can investigate the behaviour of all the basic components of an averaged description of the nuclear reaction cross-sections.

In the theoretical analysis of the cross-sections for interaction between different particles and nuclei it is common practice now to divide the reaction mechanisms into fast direct processes with the excitation of a comparatively small number of degrees of freedom in the nucleus, and slower statistical or compound processes associated with the excitation of rather complex "long-lived" states of the compound nucleus [1-4]. Reactions where one of these mechanisms is dominant are well known [3, 4]. The commonest situation, however, is when both mechanisms make commensurable contributions to the cross-sections observed. A typical example is provided by the fast-neutron scattering cross-sections considered in this paper. We hope that their discussion will not only demonstrate the potential of the existing theoretical models for describing the experimental material accumulated in the recent years but also focus the attention of experimentalists on data which it is of primary importance to refine, in the interests of further development of our ideas concerning the mechanisms of nuclear reactions and the properties of highly-excited nuclei.

1. THEORETICAL DESCRIPTION OF THE NEUTRON ELASTIC AND INELASTIC SCATTERING MECHANISMS

Optical model and direct transitions

Various modifications of the optical model of the nucleus [5-7] are used successfully at present to analyse the resonance-averaged differential particle scattering cross-sections. In the simplest phenomenological formulation of this model the interaction of the incident particle with the nucleus is approximated by the local single-particle complex potential, the imaginary part of which integrally simulates the inelastic processes accompanying elastic scattering. In the case of nucleons, the optical potential is usually selected in the form

$$V(r) = -(V_v + iW_v) f_v(r) + 4ia_s W_s \frac{df_s(r)}{dr} + V_{so} \frac{\lambda_\pi^2}{r} \frac{df_{so}(r)}{dr} (\vec{l}\cdot\vec{\sigma}), \tag{1}$$

where V_v is the depth of the real part of the potential, W_v and W_s are the amplitudes of volume and surface absorption, V_{so} is the spin-orbit component of the potential, λ_π the pion Compton wavelength and $f_i(r) = \left\{1 + \exp[(r - r_i A^{1/3})/a_i]\right\}^{-1}$ the form factors of the corresponding parts of the potential.

Solving the problem of particle scattering using the potential, we can determine a set of diagonal elements of the collision matrix or S-matrix and, with their help, find the differential $d\sigma_s(\theta)/d\Omega$ and the integral σ_s elastic scattering cross-sections for particles. In the optical model the diagonal collision matrix elements also determine the transmission coefficients

$$T_{lj}(E_n) = 1 - |S_{lj}|^2, \tag{2}$$

which characterize the probability of absorption by the nucleus of particles with a given orbital ℓ and total j angular momentum. Summing the contributions of all angular momenta, we obtain the integral compound-nucleus formation cross-section

$$\sigma_c(E_n) = \pi\lambda_n^2 \sum_{l,j} (2j+1) T_{lj}, \tag{3}$$

and adding the elastic scattering cross-section, we find the total particle-nucleus interaction cross-section

$$\sigma_t(E_n) = \sigma_s + \sigma_c = 2\pi\lambda_n^2 \sum_{l,j} (2j+1)(1 - \mathrm{Re}\, S_{lj}), \tag{4}$$

where $\lambda_n = \hbar/\sqrt{2\mu E_n}$ is the wavelength of incident particles and E_n the energy of those particles in the centre-of-inertia system. The basic equations of the optical model and the methods of their solution are given in great detail in Refs [5, 6], and many laboratories now have computer programs based on this model [7].

In earlier studies analysing the scattering cross-sections it was already noted that for medium-energy nucleons the imaginary part of the optical potential was much smaller than the depth of the real potential [5]. Under such conditions, the nucleon free-path length is comparable with the dimensions of the nucleus, and this not only makes the nucleus more "transparent" to the incident nucleon, but also increases the probability of the direct nuclear reactions occurring without the formation of a long-lived compound nucleus. In many cases, the direct-reaction cross-section can be described successfully within the framework of the distorted wave Born approximation (DWBA) [3]. The relationship of this method for the differential inelastic scattering cross-sections can be represented schematically in the form

$$\frac{d\sigma_{if}^{\lambda}(\theta)}{d\Omega} = \sum_{\mu} \left| \sum_{j_i j_f} C_{j_i j_f}^{\lambda\mu}(\theta) \int_0^\infty u_i^*(r) F_\lambda(r) u_f(r) r^2 dr \right|^2, \tag{5}$$

where $C_{j_i j_f}^{\lambda\mu}$ represents the geometrical coefficients determined by the laws of summation of the nucleon angular momenta in the entrance i and exit f channels, u(r) the radial wave functions of the optical model, and $F_\lambda(r)$ the form factor of the target-nucleus excited state.

In the phenomenological approach based on the relationship of the collective model [8] the form factors of the direct transitions are usually written in the form

$$F_\lambda(r) = \frac{\beta_\lambda R_0}{(2\lambda+1)^{1/2}} \frac{dV(r)}{dr}, \tag{6}$$

where β_λ is the amplitude of the collective excitations of a nucleus of a given multipolarity λ. Analysing the nucleon inelastic scattering cross-sections with the help of relations (5) and (6), we can study the distribution of amplitudes β_λ over the spectrum of the excited states of the nucleus. On the basis of such analysis a vast amount of spectroscopic data have now been accumulated on the collective properties of the lowest levels of nuclei [8]. However, in the case of higher levels, there are still only very meagre experimental data available on the distribution of deformation parameters $\beta_\lambda(U)$ and hence on the role of direct processes in the excitation of these levels.

Relationships (5) determine the probability of direct transitions only in the first order of the theory of perturbations. If the coupling of the entrance and exit channels is sufficiently strong, the role of the higher-order transitions will have to be taken into account when analysing the direct-reaction cross-sections. This problem can be solved most consistently by the method of strongly-coupled channels [3]. In the practical use of this method, the interaction of the incident particle with the nucleus is modelled with the help of the unified optical potential

$$V(\mathbf{r}, \xi) = V(r) + V_c(\mathbf{r}, \xi). \tag{7}$$

It also includes, apart from the single-particle optical potential (1), the potential for interaction (coupling) of channels V_c, which depends on the co-ordinates ξ of the excited states of the nuclei. Since channel coupling greatly complicates the scattering problem, we usually confine ourselves, in the analysis of experimental data, to considering the coupling of only a comparatively small number of channels corresponding to the excitation of the low-lying levels of the target nucleus. In this case, the imaginary part of the generalized optical potential (7), as in the single-channel optical model, characterizes the integral influence of all other reaction channels on the explicitly considered scattering channels.

Strong channel coupling, first of all, during the collective excitations of nuclei, and the phenomenological generalized optical potential is usually chosen in the same form as the single-particle potential (1) but with form factors $f_i(r,\Omega) = [1 + \exp\left\{(r - R_i(\Omega))/a_i\right\}]^{-1}$ depending on the collective variables: Euler angles and deformation parameters of the nucleus. For rotational axi-symmetric nuclei the corresponding radii R_i can be written in the form

$$R_i(\theta') = r_i A^{1/3} [1 + \sum_\lambda \beta_\lambda Y_{\lambda 0}(\theta')], \tag{8}$$

where θ' is the azimuthal angle with respect to the symmetry axis of the nucleus and β_λ the equilibrium deformation parameter of the nucleus. The coupling between the co-ordinate system of the deformed nucleus and the system with a fixed direction of motion of the incident particle can be found with the help of rotation functions [8]. For vibrational nuclei the radii R_i are approximated by the relations

$$R_i(\theta, \varphi) = r_i A^{1/3} [1 + \sum_{\lambda\mu} \alpha_{\lambda\mu} Y_{\lambda\mu}(\theta, \varphi)], \tag{9}$$

where θ and Φ are polar angles in an arbitrary co-ordinate system. The coefficients $\alpha_{\lambda\mu}$ are, in this case, connected with the dynamic deformation parameters β_λ by the equation

$$\alpha_{\lambda\mu} = \frac{\beta_\lambda}{(2\lambda + 1)^{1/2}} [b_{\lambda\mu} + (-)^\mu b^+_{\lambda -\mu}], \tag{10}$$

where $b^+_{\lambda\mu}$ and $b_{\lambda\mu}$ are the operators for the generation and annihilation of vibrational excitations in the target nucleus [8]. Using Eqs (8) or (9) we can expand the form factors $f_i(r,\Omega)$ in spherical harmonics and find the explicit form of the channel coupling potential (7) for the rotational and vibrational nuclei.

The equations of the unified optical model for the deformed optical potential thus introduced have been discussed by many authors, and a detailed analysis of these equations, together with references to the original works, is contained in Tamura's well-known review paper [9]. In recent years many laboratories [7, 10] have developed programs based on the unified optical model, and international nuclear data centres have done a considerable amount of work on testing and standardizing such programs [7].

On the basis of the unified optical model we can determine not only the diagonal elements of the collision matrix but also its non-diagonal elements $S^{J\pi}_{n\ell j,\, n'\ell' j'}$, which characterize the direct-excitation cross-sections for the corresponding levels:

$$\sigma^{\mathrm{dir}}_{n'} = \frac{\pi \lambda^2_n}{2(I_0+1)} \sum_{J l j l' j'} (2J+1) |S^{J\pi}_{0lj,\, n'l'j'}|^2. \tag{11}$$

Here J and π are the total angular momentum and the parity of states of the target nucleus plus nucleon system, and I_o is the spin of the target nucleus. The non-diagonal elements, together with the diagonal ones, will also enter into the determination of the transmission coefficients

$$T^{J\pi}_{nlj}(E_n) = 1 - \sum_{n'l'j'} |S^{J\pi}_{nlj,\, n'l'j'}|^2. \tag{12}$$

This relation can be used to find the transmission coefficients for not only the ground but also the excited states, and at low incident-neutron energies these coefficients may differ quite substantially [11, 12]. Knowing the transmission coefficients, we can easily find in the unified optical model the integral cross-section for absorption of particles by the nucleus or, what is practically the same, the cross-section for reactions which go through the compound nucleus stage.

Neutron scattering with compound nucleus formation

The Bohr compound nucleus model is generally used when we consider absorbed particles. It is based on the assumption that the reaction has a long-lived intermediate stage during which the nucleus "forgets" its formation conditions and then decays in accordance with statistical laws, regardless of the initial conditions of compound nucleus formation [1]. The representations of this model formulated with allowance for the laws of conservation of angular momenta and the statistical laws governing width distribution for competing decay channels of the compound nucleus are widely known as Hauser-Feshbach-Moldauer relationships [2, 13]. In the case of excitation cross-sections for isolated levels, these relationships can be written in the form

$$\sigma_{n'}^{\mathrm{comp}} = \frac{\pi \lambda_n^2}{2(2I_0+1)} \sum_{ljJ} (2J+1) \left\{ \Theta_{lj}^{J\pi}(E_n) \frac{\sum_{l'j'} \Theta_{l'j'}^{J\pi}(E_{n'}) F_{ljl'j'}^{J\pi}}{\sum_{n''l''j''} \Theta_{l''j''}^{J\pi}(E_{n''})} - \delta_{nn'} \left(\frac{\Theta_{lj}^{J\pi}}{2} \right)^2 \right\}, \tag{13}$$

where $\Theta_{\ell j}^{J\pi} = 2\pi \left\langle \Gamma_{n\ell j}^{J\pi} \right\rangle / D^{J\pi}$ are the transmission coefficients characterizing the ratio of the average partial resonance widths $\left\langle \Gamma_{n}^{J\pi} \right\rangle$ to the distance between resonances $D^{J\pi}$, and $F_{\ell j,\ell' j'}^{J\pi}$, the corrections for width fluctuation. If the distribution of partial decay widths is described by the χ_ν^2 - the distribution with ν degrees of freedom and there are no correlations of widths for the different decay channels, the correction for width fluctuation will be determined by the relation

$$F_{\beta\gamma}^{J\pi} = \left(1 + \frac{2}{\nu_\beta}\delta_{\beta\gamma}\right) \int_0^\infty dt \prod_\alpha \left(1 + \frac{2t}{\nu_\alpha} \frac{\Theta_\alpha^{J\pi}}{\sum_{\alpha'} \Theta_{\alpha'}^{J\pi}}\right)^{-(\nu_\alpha/2 + \delta_{\alpha\beta} + \delta_{\alpha\gamma})}. \tag{14}$$

The fluctuation correction increases the cross-section for elastic scattering with compound nucleus formation and, at the same time, decreases the cross-section for inelastic processes. For a small number of open channels this reduction can be very substantial [13].

Although, for calculation purposes, Eqs (8) and (9) are comparatively simple, their use for the analysis of experimental data raises a number of problems, which have not yet been fully solved theoretically. This refers, first of all, to the determination of the coupling between the transmission coefficients $\Theta_{\ell j}^{J\pi}$ and the transmission coefficients of the optical model $T_{\ell j}^{J\pi}$, and also to the problem of correlating widths in the different decay channels and determining the number of degrees of freedom $\nu_{\ell j}$. A rigorous solution of these problems as a whole is known only for the region of comparatively low incident neutron energies, which corresponds to isolated resonances in the non-averaged reaction cross-sections. Under these conditions the neutron width distribution is governed by the Porter-Thomas law ($\nu^{J\pi}_{\ell j} = 1$), and the transmission coefficients $\Theta^{J\pi}_{\ell j}$ are coupled with the corresponding optical-model coefficients by the relation

$$T^{J\pi}_{lj} = \Theta^{J\pi}_{lj} - (\Theta^{J\pi}_{lj})^2/4. \tag{15}$$

The situation turns out to be much more complex for the overlapping resonances. The coupling between coefficients $\Theta^{J\pi}_{\ell j}$ and $T^{J\pi}_{\ell j}$ can in this case be represented as

$$T^{J\pi}_{lj} = \Theta^{J\pi}_{lj} - \sum_{n'l'j'} M^{J\pi}_{nlj,n'l'j'}, \tag{16}$$

But in order to determine the terms $M^{J\pi}_{\alpha\beta}$, we now need to know the correlation properties of the resonance amplitudes of the scattering matrix [13-15]. These properties have hardly been studied at all up to now, and our ideas about them are based only on the results of statistical modelling of the neutron cross-section resonance structure [14, 15] rather than on direct experimental data. Such modelling has shown that for a fairly large number of open channels the correlation of resonance parameters can lead to an effective reduction in terms with different $M^{J\pi}_{n\ell j,\, n'\ell' j'}$. If we assume that such "cancellation" of the M terms is a general property of the region of overlapping resonances, we can directly identify the coefficients $\Theta_{\ell j}$ with the optical model transmission coefficients [15]. The question of the effective number of degrees of freedom for different decay channels, however, remains open. For overlapping resonances we do not have a rigorous determination of $\nu_{\ell j}$ and can only expect the number of degrees of freedom for the partial neutron widths to be limited by the inequality $1 \leqslant \nu_{\ell j} \leqslant 2$. On the basis of statistical modelling of cross-sections, a simple empirical relation for the effective number of channels has been suggested in Ref. [16]

$$\nu^{J\pi}_{lj} = 1 + \sqrt{T^{J\pi}_{lj}}. \tag{17}$$

It should be borne in mind that only the general trends in the variation in neutron-width fluctuations over the region of overlapping resonances are reflected fairly well by this formula and that it does not lay claim to high accuracy for a small number of open neutron channels [15].

Originally, the Hauser-Feshbach-Moldauer relationships were obtained on the assumption that the direct reaction mechanism made no contribution. Later it was shown [14, 15] that the general structure of these relationships remained unchanged also in the presence of the direct processes. In the latter case, it is only necessary to determine the transmission coefficients with allowance for the contribution of direct transitions and also to take account in the width fluctuation corrections of the correlations of widths in the channels associated with the direct transitions. These correlations will increase somewhat the fluctuation correction but this is appreciable only for a small number of open channels strongly coupled by direct transitions [15]. With an increase in the number of channels the correlation effects decrease rapidly, and the cross-sections for direct reactions and for reactions with compound nucleus formation undergo simple superposition.

On the basis of the foregoing discussion of methods of describing the nuclear reaction cross-sections averaged over the resonance structure, we can formulate a series of questions the answers to which are of topical relevance in the study of fast-neutron scattering: (1) How should the optical potential parameters be chosen for simultaneous analysis of the differential elastic and inelastic scattering cross-sections? (2) What quality should be aimed at when describing experimental data for the existing uncertainties in the parameters of the models used? (3) How unambiguous are the conclusions regarding the contribution of the direct and compound scattering mechanisms for different neutron energies at the existing uncertainties? Answering these particular questions is the main point of this review.

2. SELECTION OF THE OPTICAL POTENTIAL PARAMETERS

In using the optical model to analyse nuclear reaction cross-sections, one of two goals is generally pursued: (1) to find the best possible description of the scattering cross-sections observed for a wide group of nuclei with a single "universal" set of optical potential parameters; (2) to obtain the best possible description of the differential elastic scattering cross-sections and of the integral inelastic interaction or total reaction cross-sections for a specific nucleus and a particular incident-particle energy. Depending on how the problem is formulated, the physical content of the optical model is, of course, somewhat different. In the first case, the optical model parameters found reflect the general characteristics of variation in the single-particle average field of nuclei and the probability distribution of nucleon absorption in the nucleus, which is determined by the imaginary part of the optical potential. At the same time, with independent fitting of the optical potential parameters at each energy point the optical model acts rather as a phenomenological method of parametrizing the properties of the energy-averaged collision matrix. In this case the energy variations of the parameters and the fluctuations in the parameters of the neighbouring nuclei can not only be caused by variations in the average field but also include various structural effects associated with the individual characteristics of the nuclei.

Many authors have repeatedly searched for a universal set of optical potential parameters (see, for example, [5,6]). For neutron energies above 14 MeV, the parameters obtained by Becchetti and Greenlees from a simultaneous analysis of the differential elastic scattering cross-sections for protons and neutrons of energies up to 40 MeV have been used widely as such a set. The parametrization used by them took into account the isotopic dependence of the real and imaginary parts of the potential and the energy changes of the potential depth:

$$\left.\begin{aligned} &V_v = 56{,}3 - 24\,(N-Z)/A - 0{,}32E_n; \\ &W_v = (0{,}22E_n - 1{,}56) \ \text{or} \ 0; \\ &W_s = 13{,}0 - 12{,}0\,(N-Z)/A - 0{,}25E_n; \\ &V_{so} = 6{,}2. \end{aligned}\right\} \qquad (18a)$$

Here somewhat different geometrical parameters were taken for the real, imaginary and spin-orbit components of the potential

$$\left.\begin{array}{l} r_v^{(R)}=1{,}17;\ r_v^{(I)}=r_s=1{,}26;\ r_{so}=1{,}01; \\ a_v^{(R)}=0{,}75;\ a_v^{(I)}=a_s=0{,}58;\ a_{so}=0{,}75. \end{array}\right\} \qquad (18b)$$

All quantities in relationships (18a) are in MeV and those in (18b) in Fermi units.

Studies on the neutron differential elastic scattering cross-sections [18-26] have shown, however, that for neutron energies below 14 MeV the Becchetti-Greenlees parameters do not normally provide a satisfactory description of the cross-sections observed. In particular, for 8-MeV neutrons Holmqvist and Wiedling [18] performed a systematic analysis of the elastic scattering cross-sections for a large group of nuclei, and their description of the experimental data is shown in Fig. 1. The optical potential parmeters corresponding to this description are given in Fig. 2. It will be seen that both the geometrical parameters and the potential depths ensuring the best reproduction of the observed angular distributions fluctuate appreciably from one nucleus to another. These fluctuations do not change substantially in amplitude if in the optical potential calculations we use geometrical parameters averaged over the whole group of nuclei under consideration and there is variation only in the depth of the real and imaginary parts of the potential (see the black circles in Fig. 2). Holmqvist and Wiedling suggested the following optical potential parameters for use as the universal set in the 1.5-8 MeV neutron energy region

$$\begin{array}{l} V_v=44{,}44+0{,}1987A- \\ \quad -1{,}893\cdot 10^{-3}A^2+ \\ \quad +4{,}527\cdot 10^{-6}A^3; \\ W_s=5{,}89+ \\ \quad +9{,}376\cdot 10^{-2}A- \\ \quad -7{,}343\cdot 10^{-4}A^2+ \\ \quad +1{,}408\cdot 10^{-6}A^3; \\ V_{so}=8{,}0;\ r_v=r_{so}= \\ \quad =1{,}183+3\cdot 10^{-4}A; \\ r_s=1{,}183+4\cdot 10^{-4}A; \\ a_v=a_{so}=0{,}66; \\ a_s=0{,}48. \end{array} \qquad (19)$$

Figure 1 shows the calculations of neutron differential elastic scattering cross-sections corresponding to these parameters. Although for each specific nucleus the deviation of the experimental data from the calculated curves for the parameter set (19) is somewhat greater than for the individually chosen parameters, the single set of parameters provides, on the whole, quite a satisfactory description of the angular distributions observed. As was shown in Ref. [19], the quality of the description of the experimental elastic scattering cross-sections for 4.56 and 2.47 MeV neutron energies remains approximately the same.

Taking advantage of a more extensive set of experimental data on the elastic scattering of polarized and non-polarized neutrons, M.V. Pasechnik and co-workers [20] obtained for the same energy range ($1.5 \leq E_n \leq 6.1$ MeV) a quite different set of parameters of the average optical potential:

$$\begin{aligned} &V_v = 48{,}7 - 0{,}33E_n; \; r_v = r_s = r_{so} = 1{,}25; \\ &W_s = 7{,}2 + 0{,}66E_n; \; a_v = a_{so} = 0{,}65; \\ &V_{so} = 7{,}5; \qquad\qquad\quad a_s = 0{,}47. \end{aligned} \tag{20}$$

The difference between parameters (20) and (19) is partly due to different approaches adopted in selecting the experimental material: whereas in Refs [18,19] the authors' original measurement results were mainly used, the analysis in Ref. [20] took into account all experimental data with comparable errors. By widening the range of data analysed it is possible in many cases to bring about a substantial reduction in the influence of the systematic errors of individual measurements on the optical potential parameters obtained.

On the other hand, the difference between (19) and (20) reflects, as has been noted by many authors, the ambiguity of the procedure used in the search for the optical model parameters [5,6,18-20]. The interrelationship between changes in the energy- and geometrical parameters of the optical potential can be written usefully in the form of the integral relations

$$\mathcal{V}_v = \frac{4\pi V_v}{A} \int_0^\infty f_v(r)\, r^2\, dr; \quad \mathcal{V}_s = \frac{4\pi W_s}{A} \int_0^\infty f_s(r)\, r^2\, dr. \tag{21}$$

Parameter sets corresponding to identical values of integrals $\mathcal{Y}_V$ and $\mathcal{Y}_S$ give practically equivalent descriptions of experimental data.

The above optical potential parameters were found for the spherical optical model. At the same time, many of the nuclei analysed have low-lying collective levels, which are excited very intensively in the direct inelastic-scattering mechanism. However, at high intensities of direct transition the coupling of the elastic and inelastic scattering channels becomes substantial, and to consider this coupling we have to move on from the single-channel to the unified optical model.

In the search for the generalized optical potential parameters it is obviously best to use, as a first approximation, the spherical potential parameters found for magic nuclei. In such nuclei the effects of channel coupling are much weaker than in non-magic nuclei, and this is a very favourable condition for the study of the energy- and isotopic dependence of the potential parameters. In the case of nuclei with a closed neutron N = 50 or proton Z = 50 shell, the differential elastic scattering cross-sections for neutrons in the 7-26 MeV region have been studied in detail in Ref. [21]. From an analysis of these data and the observed energy dependence of the total neutron cross-sections for tin isotopes in the neutron energy region of up to 15 MeV the following optical potential parameters were obtained:

$$\begin{aligned} &V_v = 54{,}2 - 22\,(N-Z)/A - 0{,}32E_n; \\ &W_s = 3{,}0 - 14\,(N-Z)/A + 0{,}51E_n; \\ &W_v = 0;\ r_v = 1{,}2;\ a_v = 0{,}7;\ r_s = 1{,}25;\ a_s = 0{,}65. \end{aligned} \tag{22}$$

For the spin-orbit part of the potential the parameters taken were $V_{so} = 6.2$, $r_{so} = 1.01$ and $a_{so} = 0.75$, which were not varied during the description of experimental data. The parameters found for nuclei with a closed neutron shell (N = 50) differed from (22) only by small changes in the geometrical characteristics of the optical potential. If we compare (20) and (22) with parameter sets (18) and (19), we note, first of all, the substantial difference between the energy dependence of the imaginary part of the optical potential. As will be shown below, correct determination of this dependence is extremely important in the analysis of the part played by the direct processes at neutron energies below 7 MeV.

The main differences between the descriptions of neutron differential elastic scattering cross-sections in the spherical and unified optical models can be demonstrated with the help of the results shown in Fig. 3. The calculations given here for the two models were made with the same set of optical potential parameters:

$$\begin{aligned}&V_v=51{,}85-24\,(N-Z)/A-0{,}33E_n;\ W_s=2{,}55\sqrt{E_n};\\&W_v=0;\ W_{so}=7{,}0;\\&r_v=r_s=r_{so}=1{,}25;\ a_v=a_{so}=0{,}65;\ a_s=0{,}48,\end{aligned}\qquad(23)$$

and, in the case of the unified optical model, the dynamic deformation parameters β_λ for the low-lying quadrupole and octupole excitations are based on available experimental data on direct reactions and on the Coulomb excitation of the low-lying levels of the even-even nuclei [22]. For odd nuclei these calculations used the model for weak coupling of the odd particle with the collective quadrupole phonons of the even-even core [8].

A comparison of Figs 1 and 3 suggests that for the even-even S, Cr, Fe, Ni and Zn nuclei, in which the relationships of the phenomenological collective model reproduce the properties of the low-lying collective levels relatively well, the description of experimental data in the unified optical model with a single parameter set (23) is approximately the same as in the spherical optical model with individually fitted parameters. A similar conclusion will be valid also for the odd Cu and Nb nuclei in which the weak coupling model is in fair agreement with the observed low-lying-level schemes. At the same time, the weak coupling model much less satisfactorily reproduces the experimental spectra of levels in the Mn, Co and As isotopes, and from the data in Fig. 3 we can see that it is for these isotopes that the description of the angular distributions in the channel-coupling model adopted is less satisfactory than in the case of individual fitting of the optical potential parameters (Fig. 1).

In recent years the strongly coupled channel method has increasingly been used in practice for neutron cross-section analysis, and numerous examples of a description of neutron differential elastic scattering cross-sections obtained by this method are given in Refs [25-27]. In spite of a certain amount of scatter in the optical potential parameters obtained by such analysis, it can be concluded, by and large, that the parameters obtained by the strongly coupled channel method fluctuate much less from one nucleus to another than the individual sets of parameters of the spherical optical model. Moreover, the parameters of the real part of the optical potentials (22) and (23) also show much better agreement than similar parameters for single-channel optical analysis (see Fig. 2) with the conventional parameters of the single-particle potential of the shell model. The fact of this agreement is one of the most important achievements of the unified optical model.

3. DIFFERENCES IN DYNAMIC DEFORMATION PARAMETERS IN NUCLEON INELASTIC SCATTERING REACTIONS AND IN COULOMB EXCITATION OF NUCLEI

At incident-neutron energies above 7 MeV in medium and heavy nuclei the total number of open channels for compound nucleus decay is so high that scattering with compound nucleus formation does not make any appreciable contribution to the observed excitation cross-sections for low-lying levels. Under these conditions, the inelastic scattering cross-sections for the low-lying levels are determined fully by the direct transitions, and their analysis provides an effective means of studying the collective excitation characteristics of nuclei.

The bulk of data on the collective properties of nuclei are obtained at present from an analysis of the Coulomb excitation of low-lying levels. In accordance with the representations of the collective model of the nucleus, the reduced probability of the corresponding electrical γ-transitions is connected with the dynamic deformation parameters of the nucleus (10) by the relationship

$$B(E\lambda, 0^+ \rightarrow \lambda^\pi) = [(3/4\pi)\, ZeR_0^\lambda]^2 \beta_\lambda^2. \qquad (24)$$

The systematics of the deformation parameters obtained on the basis of this expression have been discussed in many studies [28,29]. It is ordinarily assumed that the same parameter values also determine the direct reaction cross-sections for particle inelastic scattering at the low-lying collective levels. This asumption is not strict enough from the standpoint of the microscopic approach since it makes no allowance for differences in the excitation of the isoscalar and isovector components of the form factors for nuclear transitions. The nature of such differences can be investigated easily if we take as an example the valency transitions in the simplest shell model of the nucleus.

In the case of nuclei with a filled neutron shell, low-frequency excitations can be formed only from proton transitions, and since two-particle effective forces for non-identical nucleons are noticeably greater than those for identical nucleons, the form factors of the direct transitions in such nuclei should be much greater for the (n,n') than for the (p,p') reaction, whereas nuclei with a closed proton shell should exhibit the opposite picture. This is a simplified example, and in actual nuclei the valency transition intensity is influenced considerably by the polarization of nucleons in the filled shells. However, the main qualitative features of the above-mentioned differences in the form factors of the proton and neutron inelastic scattering reactions remain unchanged if allowance is made for the polarization effects. In Ref. [30] a quantitative analysis was performed of the differences expected, in this case, in the dynamic deformation parameters for electromagnetic excitations of nuclei and nucleon inelastic scattering reactions.

The theoretically predicted differences in the nuclear and electromagnetic deformation parameters have received confirmation as a result of the recent high-precision studies of an experimental nature on the neutron inelastic scattering cross-sections for near-magical nuclei [21,31]. The authors of the relevant papers measured with high accuracy the neutron differential elastic and inelastic scattering cross-sections at 11 MeV in the ^{88}Sr, ^{90}Zr and ^{92}Mo nuclei, which have a closed neutron shell N = 50, and also in the tin isotopes $^{116,\ 118,\ 120,\ 122,\ 124}Sn$, which correspond to a closed proton shell Z = 50. The tin isotope measurements are given in Fig. 4, together with a theoretical description of the cross-sections observed [31]. By analysing the elastic scattering cross-sections the authors were able to determine fairly reliably the optical potential parameters for each of the nuclei considered, while the subsequent description of inelastic scattering cross-sections by the distorted wave Born approximation enabled them to determine the quadrupole deformation parameters $\beta_2^{(n)}$. The deformation parameters thus found are given in Table 1, which also contains the experimental values of the deformation parameters $\beta_2^{(p)}$, and $\beta_2^{(\gamma)}$, obtained respectively from an analysis of the proton inelastic scattering cross-sections and from the description of Coulomb excitations of nuclei. Although in many cases the errors of the deformation parameters obtained are commensurate with the expected differences in the parameters themselves, the available data, as a whole, still point quite reliably to a systematic difference in the parameters $\beta_2^{(n)}$, $\beta_2^{(p)}$ and $\beta_2^{(\gamma)}$; these differences are in satisfactory agreement with the theoretical analysis of the nuclear and electromagnetic deformation parameters shown in Table 1.

The above theoretical evaluations of the dependence of the dynamic deformation parameters on the mode of excitation of the nucleus were obtained on the basis of the simplest schematic model of polarization effects, where all high-frequency excitations of the core are concentrated in two collective modes - isoscalar and isovector quadrupole giant resonances [30]. The defects of this approximation can be eliminated if the form factors of the nuclear transitions are analysed with the use of more realistic microscopic models. Such an analysis was performed for the effective interaction of nucleons, which is represented in the form of separable multipole forces consistent with the actual average field of nuclei [32]. These forces are utilized widely to describe the collective properties of nuclei [8], and can be used quite satisfactorily to reproduce all the basic characteristics of the observed spectral intensity distributions of low- and high-frequency excitations. The values of the deformation parameter ratio $\beta_2^{(n)}/\beta_2^{(p)}$ obtained in this analysis were 1.08-1.12 for nuclei with N = 50 and 0.90-0.94 for the tin isotopes [32]. Although these figures are somewhat lower than the evaluations of the schematic model (see Table 1), the total effect of the systematic difference in the quadrupole deformation parameters in the groups of nuclei considered remains very stable during variations in the theoretical description.

As we move away from the magic numbers, we should expect a decrease in the shell effects and a corresponding diminution of differences in the dynamic deformation parameters for the different fields which induce nuclear transitions. Since this always augments the absolute value of the deformation parameters, the study of the dependence of deformation parameters on the inducing field, in the case of non-magic nuclei, is experimentally a very complex problem. The main difficulties involved in solving this problem can be demonstrated by the example of the study made in Ref. [33], where the elastic and inelastic scattering cross-sections for 6, 8 and 10 MeV neutrons for the $^{76, 78, 80, 82}$Se isotopes were measured and analysed. Initial analysis of these data within the framework of the spherical optical model and the distorted wave Born approximation for the inelastic channel showed that, although the description of the observed cross-sections might be fairly good, the parameters derived here were too unrealistic. The isospin dependence of the real part of the optical potential is almost twice as weak as that obtained for the neighbouring nuclei (22), while the quadrupole deformation parameters are several times greater than in the description of the Coulomb excitation.

The above-mentioned inconsistencies can be overcome to a considerable extent if we analyse the elastic and inelastic scattering cross-sections by the coupled-channel method. For an incident-neutron energy of 8 MeV the description of experimental data by this method is given in Fig. 5, and the corresponding quadrupole deformation parameters in Table 2, together with the parameters found in the analysis of proton inelastic scattering [34] and with the experimental data on electromagnetic excitation of nuclei [35]. As follows from the results of proton studies, in the selenium isotopes we have differences in the nuclear and Coulomb deformation parameters of the same sign $\beta_2^{(\gamma)} > \beta_2^{(p)}$ as in the nuclei considered above with the filled neutron shell N = 50. Here the $\beta_2^{(\gamma)}/\beta_2^{(p)}$ ratio increases as the shell fills, approaching the values given in Table 1. On the basis of available data it is still difficult to see what conclusions should be drawn from the neutron experiment results. Apart from having the statistical errors of analysis shown in Table 2, the derived parameters $\beta_2^{(n)}$ may also be somewhat distorted by systematic errors associated with the choice of the optical potential. In order to eliminate such errors, we need to study the neutron differential inelastic scattering cross-sections over a wider range of incident-neutron energies, and it is evident that only on the basis of such studies can we conclude what the differences between $\beta_2^{(n)}$ and $\beta_2^{(p)}$ really are.

The foregoing consideration was concentrated entirely on the quadrupole deformation parameters, which determine the direct excitation intensities of the lower 2^+ levels of even-even nuclei. A similar dependence of the dynamic deformation parameters on the inducing external field can be expected likewise during direct excitation of higher levels or of levels of a different multipolarity. By now relatively extensive experimental data have been accumulated on direct excitation during the scattering of various particles of the first octupole levels of even-even nuclei [8,29, 35,36]. Unfortunately, the errors of the octupole deformation parameters derived in thismanner are in most cases still too high to be used as a basis for drawing any obvious conclusions concerning differences in the nuclear and Coulomb deformation parameters. Experimental data on transitions of high multipolarity $\lambda \geqslant 4$ are scanty. Although no systematic theoretical analysis has yet been made of such transitions, from the general concepts of the microscopic approach we can expect that in the case of the corresponding comparatively weakly collectivized levels the differences in the effective dynamic deformation parameters for different particles will be much greater than for the lowest strongly collectivized quadrupole and octupole levels. Experimental studies on these differences would be of considerable interest in the study of the multipole excitation structure of nuclei and in the analysis of the integral contribution of direct transitions in different nuclear reactions.

4. ANALYSIS OF THE NEUTRON DIFFERENTIAL INELASTIC SCATTERING CROSS-SECTIONS FOR LIGHT NUCLEI

In the foregoing we considered nuclei where, at incident-neutron energies above 6 MeV, the direct mechanism of low-level excitation is dominant. If at the same energies we move on to lighter nuclei, not only the direct scatter mechanism but also scattering with compound nucleus formation becomes substantial. Analysing the angular distributions of the scattered neutrons, we can study the energy dependence of the contributions made by both mechanisms. For this purpose, the mass number region $20 < A < 40$ is especially favourable since it is simpler here than in medium and heavy nuclei to separate experimentally the excitation functions for discrete levels, while the observed neutron cross-sections still remain averaged over a sufficiently large number of compound-nucleus resonances.

Of the light nuclei, the one which has been investigated in greatest detail is the isotope ^{28}Si, for which measurements and analysis of the neutron differential elastic and inelastic scattering cross-sections for the first 2^+ level ($Q = -1.779$ MeV) in the 6-15 MeV incident energy region were performed by the authors of Refs [37-44], and the excitation cross-sections for higher levels were also studied in Refs [43,44]. The observed neutron elastic scattering cross-sections and their theoretical description are given in Fig. 6 [44]. Similar data on the neutron-inelastic scattering cross-section for the 2^+ level are given in Fig. 7 and on the inelastic scattering cross-sections for 4^+ ($Q = -4.618$ MeV) and 0^+ ($Q = -4.979$ MeV) levels in Fig. 8.

The theoretical analysis of the scattering cross-sections first involved a study of the possibility of describing the experimental data on the basis of the spherical optical model. For this purpose, use was made of the optical potential parameters found in the description of the neutron differential elastic scattering cross-sections at 10 MeV [41]. From the calculation results given in Fig. 6 it will be seen that these parameters can be used to obtain a fairly satisfactory description of the observed elastic scattering cross-sections for the entire incident-neutron energy region from 7 to 14 MeV. Difficulties arise, however, during use of the given optical potential in the analysis of the inelastic scattering cross-sections. On the one hand, for a description based on the distorted wave Born approximation of the direct excitation cross-sections for the first 2^+ level in the region $E_n > 10$ MeV we require extremely high values of the quadrupole deformation parameters [41]. At the same time, for lower energies the cross-section for inelastic scattering with compound nucleus formation is on the high side, a fact which comes out especially clearly during analysis of the excitation cross-sections for the 4_1^+ and 0_2^+ levels [44].

If we move on to the strongly-coupled channel model, we have first to reduce the imaginary part of the optical potential in order to describe the experimental data. These changes characterize the role of the inelastic reaction channels considered in the redistribution of the incident-neutron flux, and the depth of the imaginary part of the potential decreases the more strongly, the greater the number of channels included in the coupling scheme. In the calculations we took the 0_1^+-2_1^+-4_1^+ rotational level-coupling scheme, to which we added the 0_1^+-0_2^+ vibrational level-coupling scheme. This required reducing the imaginary part of the optical potential by almost half. The description thus obtained for the angular distributions of the inelastically scattered neutrons differs, on the whole, only very slightly from a description based on the spherical optical model (see Fig. 6). Of substantially greater importance is the consistency to be found in the strongly-coupled channel model in the case of the results of neutron inelastic scattering cross-section analysis. Because of the decrease in the imaginary part of the potential there was a corresponding decrease in the cross-sections for neutron elastic and inelastic scattering with compound nucleus formation, and this agrees satisfactorily with the experimental data at 7 and 8 MeV neutron energies, where we observe a considerable contribution by the compound scattering mechanism.

It should be noted that for 7-8 MeV neutrons, by analysing the differential elastic scattering cross-sections in the region of the deepest minimum ($\theta \approx 110^{\circ}$), it is possible to study the role of resonance overlapping in the description of the correction for neutron width fluctuation (14). The cross-section at the minimum is determined almost entirely by the mechanism of scattering with compound nucleus formation, and by analysing the observed cross-sections we can find the average value of the correction $\overline{F}$ for the elastic channel. Since the total number of open channels for compound nucleus decay at the energies considered is sufficiently large, the corresponding correction should approach its maximum values: $F_{nn} = 3$ in the absence of correlation of the resonance parameters, and $F_{nn} = 2$ for the strongly overlapping correlated resonances [13-15]. The value of the correction $\bar{F}_{nn} \approx 1.6\text{-}1.8$ [40] required to describe the experimental data is very close to the expected average value of the correction for strongly overlapping resonances; this result is the experimental confirmation of the need to take into account the correlation of the resonance parameters when calculating the average neutron reaction cross-sections. The required fluctuation increase in the elastic scattering cross-section is reproduced satisfactorily in the calculations using Eq. (17) to determine the number of open channels, and this can serve as an additional proof of the effectiveness of such a simple modelling of the statistical properties of neutron widths.

In calculations of the neutron direct inelastic scattering cross-sections a very important problem is the choice of the deformation parameters which determine the form factors (8) for direct excitation of collective levels. The rotational nature of the lowest levels of the ^{28}Si nucleus is usually identified on the basis of the observed intensity of E2 transitions [45] and also on the basis of analysis of charged-particle differential inelastic scattering cross-sections [46-49]. However, the derivation of the equilibrium deformation parameters here is very ambiguous. The reason for this situation can be understood easily from the description, given in Fig. 9, of the scattering cross-sections for 10 MeV neutrons at 0^+, 2^+ and 4^+ rotational band levels. The theoretical curves were obtained for two sets of parameters β_2 and β_4 corresponding to the elongated "cigar-shaped" ($\beta_2 > o$) and the flattened "lenticular" ($\beta_2 < o$) shape of the nucleus. Neither the elastic scattering cross-section nor the angular distributions of inelastic scattering of neutrons at the first 2^+ level is critical for the choice of the equilibrium deformation sign, and only the data on the excitation of the 4^+ level enable us, to some extent, to distinguish between the alternative sets of parameters considered.

Since a similar conclusion is valid also for the charged-particle differential scattering cross-sections, the data on the asymmetry of polarized proton scattering were used in Refs [47,48], in addition to the inelastic scattering cross-sections, in order to determine the deformation parameters. Simultaneous analysis of these data yielded values of the parameters $\beta_2 = -0.55$ and $\beta_4 = 0.33$ [47] for the incident-proton energy of 20.3 MeV, and $\beta_2 = -0.40$ and $\beta_4 = 0.10$ [48] for the proton energy of 24.5 MeV. In Ref. [49] the data on the probability of proton spin reversal during scattering have been analysed, together with the inelastic scattering cross-sections, for the 14-40 MeV incident-proton energy region. The hexadecapole deformation parameters found in this manner depend quite strongly on proton energy - their values varied from $\beta_4 \approx 0.35$-0.40 for 14 MeV protons to $\beta_4 = 0.15$ for high-energy protons. The quadrupole deformation parameters varied much less strongly - from $\beta_2 = -(0.4$ to $0.5)$ in the proton energy region below 20 MeV to $\beta_2 = -(0.37 \pm 0.05)$ for high-energy protons.

The energy dependence of the deformation parameters obviously reflects the drawbacks of the rigid rotator model used in analysis of the experimental data. The observed ratio of the rotational band energy levels $E_{4+}/E_{2+} = 2.59$, just as the ratio of the reduced probabilities of E2 transitions $B(E2; 4^+ \rightarrow 2^+)/B(E2; 2^+ \rightarrow 0^+) = 1.06 \pm 0.14$ [45], differs appreciably from the values corresponding to the rigid rotator model: $(E_{4+}/E_{2+})^{rot} = 3.33$ and $B(E2; 4^+ \rightarrow 2^+)/B(E2; 2^+ \rightarrow 0^+) = 1.43$. Disregarding these differences in the analysis of particle inelastic scattering cross-sections, we obtain somewhat distorted values of the deformation parameters, and the energy changes in the parameters characterize the possible distortions.

The influence of deviations from the channel coupling scheme of the rigid rotator model on neutron differential inelastic scattering cross-sections was studied in Refs [43,44], where it was found that weakening of the coupling of the 2_1^+ and 4_1^+ levels with simultaneous increase in the hexadecapole deformation parameter led to a general improvement in the description of the observed angular distributions of neutron scattering at levels 2_1^+ and 4_1^+ for the entire incident-neutron energy region from 7 to 14.8 MeV. The absolute values of the deformation parameters $\beta_2 = 0.48$ and $\beta_4 = -0.30$ thus obtained are close to the values derived from the differential scattering cross-sections for protons of comparable energies [47,49]. The signs of the deformation parameters were chosen on the basis of an analysis of excitation cross-sections for the 4_1^+ level but in view of the ambiguities of the analysis referred to above, no great value should be attached to this choice. Given the existing neutron cross-section errors, not all the parameters of the optical potential can yet be determined, and the deformation parameter values found actually contain possible errors in determination of the remaining parameters. These errors can be eliminated by improving the reliability with which the neutron differential elastic and inelastic scattering cross-sections are measured, i.e. by obtaining experimental data comparable in accuracy to the data given in Figs 4 and 5.

The existing ambiguities in the choice of parameters for the unified optical model are, however, not very substantial for the determination of the ratio of the contributions of the direct and compound scattering mechanisms to the neutron cross-sections under study. From the data presented in Figs 7 and 8 it will be seen that direct scattering becomes dominant at neutron energies above 8 MeV for the 2_1^+ and 0_2^+ levels and at those above 10 MeV for the 4_1^+ level. In the case of the 2_1^+ level the observed integral inelastic scattering cross-sections for neutron energies below 10 MeV are shown in Fig. 10. The measurements by the different experimental groups [37-44, 50-53] show a fair agreement within the errors given. By analysing the observed asymmetry of the angular distributions for scattered neutrons we can investigate the contribution of the direct transitions right to the neutron energy of 3 MeV. If we consider together the entire set of experimental data on the angular distributions of neutrons elastically and inelastically scattered at level 2_1^+, the best description of the observed cross-sections is given by the strongly-coupled channel model with optical potential (20), where, making allowance for the 0_1^+-2_1^+ level coupling (β_2 = 0.48), the imaginary part is reduced by 20%, i.e. we take $W_s = 5.7 + 0.52E_n$. Figure 10 gives for this choice the corresponding parameters of the integral direct and compound scattering cross-sections for neutrons at the first 2^+ level. When parameter set (23) is used, the direct scattering cross-section in the region E_n < 6 MeV is too high. This drawback can be easily overcome by changing the energy dependence of the imaginary part of the potential (23), and with identical choice of the imaginary potential the parameter sets (20) and (23) become practically indistinguishable. If we increase the number of coupled levels, it is necessary to reduce still further the imaginary part of the optical potential, by reducing, in this case, mainly the first term in the parametrization of W_s used and by leaving the energy dependence without any substantial changes. Such a dependence is required, in particular, to describe the angular distributions given in Figs 6-8.

If we go over to the neutron energy region below 3 MeV, experimental determination of the average cross-sections becomes the main problem of analysis. The experimental data clearly show the fluctuation structure of the neutron cross-sections (Fig. 11). Since the amplitude of the observed fluctuations is determined mainly by the resolution of neutron spectrometers, it is a quite complicated problem to correct the observed cross-sections and the average cross-sections obtained on their basis for the resonance absorption of neutrons in the target. It is still more complicated to plot the fluctuation-averaged angular distribution of elastically and inelastically scattered neutrons, and at present we simply do not have enough experimental data for a plot of this kind. Yet by comparing the available set of data with the optical model calculations we can conclude that the theoretical description is in qualitative agreement with experiment (see Fig. 11). For purposes of a more rigorous quantitative analysis of the data and to verify the applicability of the various sets of optical potential parameters, we need higher-precision measurements of the angular distributions of neutron elastic and inelastic scattering.

The direct mechanism by which there is excitation of the lowest levels over a wide range of excitation energy was also studied in the ^{32}S nucleus [37-41, 50,57]. For neutron energies above 7 MeV, the observed neutron differential inelastic scattering cross-sections for the 2_1^+ level (Q = -2.23 MeV) are given in Fig. 12, together with the results of theoretical description of the cross-sections [57]. The optical potential parameters in the given description were determined from an analysis of the differential elastic and inelastic scattering cross-sections for 8 and 9 MeV neutrons [39], and no changes were required in the parameters in the case of a comparatively minor broadening of the range of incident-particle energy. Since the spectrum of the low-lying levels of the ^{32}S nucleus corresponds quite satisfactorily to the representations of the vibrational model, the calculation of direct transitions in the strongly-coupled channel model was based on the 0_1^+-2_1^+ vibrational level coupling scheme and on the same dynamic deformation parameter $\beta_2 = 0.30$ as in the description of charged-particle inelastic scattering cross-sections [48].

Similar experimental data on and results of theoretical description of neutron scattering cross-sections for the 2_1^+ level (Q = -1.369) of the ^{24}Mg nucleus are given in Fig. 13 [58]. The 0_1^+-2_1^+ rotational level coupling scheme and equilibrium deformation parameters $\beta_2 = 0.55$ and $\beta_4 = 0.05$ were used in the calculations. Since the ratio of the rotational band energy levels $E_{4+}/E_{2+} = 3.02$ is closer to the predictions of the rigid rotator model in the ^{24}Mg nucleus than in Si, the differences in the equilibrium deformation parameters of the nucleus obtained in the different experiments are substantially smaller [45-47]. Given the existing errors in the experimental data, it is not, however, possible to decide whether these differences are due to ambiguities in the choice of the optical potential parameters or whether they characterize the actual difference in the isovector intensity components for direct excitation of levels during the scattering of the different particles.

From the calculations of the cross-sections for the direct and compound mechanisms of scattering given in Figs 7, 12 and 13 it will be seen that the contribution of the two mechanisms to the observed excitation cross-sections for the first 2^+ level becomes approximately identical at 7-9 MeV neutron energies. At higher energies direct excitation dominates, and the integral scattering cross-section varies comparatively slowly with growth in neutron energy. Although at neutron energies below 7 MeV the behaviour of the excitation functions is determined mainly by scattering with compound nucleus formation, we cannot, however, neglect the contribution of direct transitions in the description of scattering cross-sections at collective levels over the entire energy range right up to the threshold (see Fig. 10).

In order to make a fuller study of the role of direct transitions in the region of the maximum of the excitation functions for the low-lying levels, Schweitzer and co-workers [59] performed systematic measurements of the differential elastic and inelastic scattering cross-sections for the first levels of even-even and odd light nuclei for neutrons with an initial energy of 3.4 MeV. Pairs of neighbouring even-even and odd nuclei were measured simultaneously in order to eliminate possible systematic experimental errors. Under these conditions the relative behaviour of the differential scattering cross-sections for a given pair of nuclei is determined with a much smaller error than in the case of the absolute cross-sections, which include not only the statistical measurement error but also errors in the corrections made for attenuation and multiple scattering of neutrons in the samples, for the efficiency of the neutron spectrometer and so on. The observed angular distributions of the elastically and inelastically scattered neutrons are given in Figs 14 and 15, together with a theoretical description of the cross-sections. Table 3 presents the integral inelastic scattering cross-sections obtained for the entire group of light nuclei studied.

Theoretical calculations were performed in the strongly-coupled channel model with allowance for the rotational coupling of levels $0_1^+-2_1^+$ for even-even nuclei and coupling of the ground state I_o^π with the whole multiplet of levels $(I_o^\pi \otimes 2^+)$ for odd nuclei. Here the spin-orbit splitting of the reaction channels was neglected in odd nuclei in order to reduce the number of coupled equations. The equilibrium deformation parameters were the same as those in the description of higher-energy neutron scattering (β_2 = 0.55 for ^{23}Na and ^{24}Mg, β_2 = 0.48 for ^{27}Al and ^{28}Si), and the parameter set (19) was used for the optical potential. With the use of even-even nuclei as an example it was, however, verified that approximately the same description of the observed differential cross-sections could be obtained for the parameter set (20) and also for the parameters employed to describe the differential scattering cross-sections for 7-12 MeV neutrons if the imaginary part of the potential was reduced by about 20%.

On the whole, the calculation results agree quite satisfactorily with the observed neutron differential elastic scattering cross-sections (see Fig. 14) but much less satisfactorily with the inelastic scattering cross-sections (see Fig. 15). The calculated integral cross-sections for inelastic scattering with compound nucleus formation are always smaller than the experimental cross-sections (see Table 3), and this indicates, in the same way as the observed total asymmetry of angular distributions of inelastically scattered neutrons, that the direct mechanism of scattering for most levels makes a substantial contribution. The "fluctuations" in angular distributions are still unclear (see Fig. 15). At present, it is difficult to decide whether they are due to errors disregarded in the experimental data or whether they reflect actual fluctuations of differential cross-sections associated with the limited range of the averaged resonances of the compound nucleus.

5. ANALYSIS OF THE EXCITATION FUNCTIONS FOR THE LOW-LYING LEVELS OF MEDIUM NUCLEI

The general features of the energy dependence of the contributions made by the direct and compound neutron scattering mechanisms, which we have discussed above, are also found in heavier nuclei. Since the level density of the compound nucleus rises with increase in the mass number, the fluctuations in the behaviour of the average cross-sections become weaker, and for most medium and heavy nuclei the relationships of the statistical theory ought to describe satisfactorily the differential and integral excitation functions for isolated levels over the entire energy range, right up to the threshold. By analysing the corresponding experimental data we can study the role of direct transitions and the energy dependence of the optical transmission coefficients in the region of comparatively low outgoing-neutron energies. We discuss the results of these studies for nuclei of the iron group - the ones for which most detailed experimental data have now been accumulated.

Figure 16 shows the differential elastic and inelastic scattering cross-sections for the first 2^+ level of the ^{52}Cr nucleus in the case of 5, 6 and 7 MeV neutrons [60]. It also gives the results of a theoretical description of the cross-sections with the set of optical potential parameters (20). As in similar calculations for light nuclei, the amplitude of the imaginary part of the potential (20) in the strongly-coupled channel model was reduced by about 20%, and the quadrupole deformation parameter $\beta_2 = 0.23$ was determined from the data on the Coulomb excitation of levels [28]. Such a choice of parameters ensures a satisfactory description of the asymmetry observed in the angular distributions of inelastically scattered neutrons, and this enables us to determine the contribution of direct transitions with sufficient reliability (see Fig. 16). The contributions made by the direct mechanism of inelastic scattering and scattering with compound nucleus formation are approximately identical at 6 MeV incident-neutron energy. With a decrease in energy the integral cross-section for direct transitions does not increase significantly, whereas the cross-section for the compound mechanism of scattering exhibits comparatively rapid growth.

The measurements of the neutron integral inelastic scattering cross-sections for the first 2^+ level of ^{52}Cr are presented in Fig. 17. The large scatter of experimental points at neutron energies below 3 MeV is due, first of all, to the errors in the methods of measurement used by the different authors and not to fluctuations in the average cross-sections. Improved experimental procedures have partially eliminated this error, and the results of later measurements generally tally much better than did the initial experimental data [60]. The observed energy dependence of the inelastic scattering cross-sections is described satisfactorily by the theoretical curve, obtained for the optical potential parameters (20), which takes into account not only neutron scattering with compound nucleus formation but also the incoherent contribution of direct transition [60].

A similar analysis of experimental data on the differential and integral cross-sections for excitation by neutrons of the lowest levels of the even-even ^{56}Fe, ^{58}Ni and ^{60}Ni nuclei was made also by the authors of Refs [22, 65-67]. The conclusions reached by them regarding the contribution of direct transitions and the choice of the optical potential parameters did not differ substantially from the results obtained for ^{52}Cr. If we compare the excitation function for the first 2^+ level in ^{52}Cr (see Fig. 17) and ^{28}Si (see Fig. 10) nuclei, we see that the energy dependences of the direct and compound components of the inelastic scattering cross-sections in light and medium nuclei are qualitatively similar. The observed quantitative differences in the direct scattering cross-sections are due to the higher values of the quadrupole deformation parameters of the light even-even nuclei, while the faster reduction in the cross-section for scattering with compound nucleus formation with increase in neutron energy in medium nuclei reflects a general build-up of the excited level density.

Figure 17 also shows the experimental data on the excitation function for the 4_1^+ level of the ^{52}Cr nucleus. The relationships of the statistical theory give quite a good description of the observed integral scattering cross-sections in the neutron energy region from threshold to 7 MeV, and it is only in the region of higher energies that the contribution of direct transitions has to be taken into account.

Systematic studies on the role of direct transitions at 3.4 MeV neutron energies were performed in Ref. [68] for a number of neighbouring even-even and odd nuclei of the iron group. The measured neutron differential elastic scattering cross-sections for the ^{51}V, ^{55}Mn, ^{56}Fe and ^{59}Co nuclei are given in Fig. 18 and the neutron inelastic scattering cross-sections for the low-lying levels of the ^{51}V, ^{56}Fe and ^{59}Co nuclei in Figs 19 and 20. The differential inelastic scattering cross-sections obtained for ^{55}Mn are substantially similar to those for ^{51}V [68]. The energy resolution of the spectrometer (about 100 keV) did not permit separation of inelastic scattering at the first excited level $7/2^-$ (Q = -0.126 MeV) of the ^{55}Mn nucleus from the elastic scattering peak, and for this nucleus Fig. 18 shows the sum of the cross-sections for elastic scattering and scattering at level $7/2^-$. For the same reason, the measured inelastic scattering cross-sections for the ^{59}Co nucleus are the sum of the scattering cross-sections for three levels $3/2^-$, $9/2^-$ and $3/2^-$ with energies 1.099, 1.190 and 1.291 MeV, respectively, and also for levels $1/2^-$, $11/2^-$ and $5/2^-$ with 1.434, 1.460 and 1.471 MeV (see Fig. 20).

The theoretical description of the observed cross-sections was performed in the strongly-coupled channel model for the $0_1^+-2_1^+$ vibrational level coupling scheme in the ^{56}Fe nucleus and the equivalent scheme of coupling the ground state I_o^- with the multiplet of levels $(I_o^- \otimes 2^+)$ in odd nuclei. Here use was made of the optical potential parameters (19) and the values of the dynamic deformation parameters β_2 = 0.23 for the ^{51}V and ^{55}Mn nuclei and β_2 = 0.211 for ^{59}Co. The spin-orbit splitting of the scattering channels was disregarded in order to reduce the calculation time for odd nuclei. The calculation results show sufficiently satisfactory agreement with the measured neutron differential elastic and inelastic scattering cross-sections. The integral inelastic scattering cross-sections obtained are given in Table 4, where the last column but one shows the contribution of the compound mechanism of scattering corresponding to the statistical model parameters mentioned above. For most of the levels considered the observed inelastic scattering cross-sections exceed the calculated values of the cross-sections for neutron scattering with compound nucleus formation and, apart from the asymmetry of the angular distributions of scattered neutrons, this result demonstrates the substantial contribution of the direct processes. The evaluations of this contribution are presented in the last column of Table 4 [68]. It will be seen that for levels of odd nuclei with high spin values the role of direct transitions is very considerable and cannot be disregarded in the description of the excitation functions for such levels.

It should be noted that for the ^{56}Fe nucleus the angular distributions of inelastically scattered neutrons at incident energies below 3.5 MeV were also studied in Refs [69-71]. Comparing the results of these studies, we find considerable differences in the evaluations of the contribution by direct transitions. These differences are due, firstly, to differences in the observed asymmetry of angular distributions of scattered neutrons and, secondly, to differences in the optical potential parameters. Analysis of high-resolution experiments showed [71] that certain fluctuations in the energy dependence of the cross-sections persisted even after averaging over a 200 keV interval and, consequently, that the differential cross-sections measured at discrete energy points could still not be identified with the optical average cross-sections. If, in selecting the optical potential parameters, we seek to describe the inelastic scattering cross-sections in a wide energy region [22,65], we get for ^{56}Fe approximately the same evaluation of the integral direct inelastic scattering cross-section as for ^{52}Cr (see Fig. 17). If, therefore, we use the parameter set (20) or (22) to describe the excitation functions for the low-lying levels of odd nuclei, we shall obtain for 3.4 MeV neutron energy direct transition contributions 1.5-1.8 times higher than those given in Table 4. For the purpose of a more reliable analysis of the role of the direct processes it would be of considerable interest to make precision measurements of the neutron differential scattering cross-sections for levels of odd nuclei with spins $I_f^\pi > I_o^\pi$.

When describing the low-energy sectors of the excitation functions for isolated levels, a very important problem is the consistency of the optical model parameters with the experimental values of the neutron strength functions. The spherical optical model with the optimum optical-potential parameters (19) or (20) reproduces only the global dependence of the neutron strength functions on mass number [5,9]; however, in the case of specific nuclei, the observed strength functions differ very substantially from the optical model predictions. The experimental and calculated values of the strength functions for nuclei of the iron group, given in Table 5, can serve as an example of these differences. Although the description of experimental data can, on the whole, be improved by going over from the single-channel optical model to the coupled-channel model, the differences between calculation and experiment even in the strongly-coupled channel model are still considerable for many nuclei. Similar differences were discussed in Refs [72-74] for a wider group of nuclei. An interpretation of these differences may be sought in the theory of doorway states [75] or in any other formulations of the microscopic theory of nuclear reactions [76]; however, whether or not there exists a more fundamental explanation for the nature of the observed effects, the experimental values of the strength functions should undoubtedly be taken into account in the phenomenological analysis of the excitation functions for the low-lying levels of specific nuclei.

The role of neutron strength functions in the description of the near-threshold behaviour of the excitation functions for the first levels of even-even nuclei can be seen from the results presented in Fig. 21. Calculations with transmission coefficients $T_{\ell j}(E_n)$ corresponding to the spherical optical model give a substantially higher value of the neutron inelastic scattering cross-section for the first 2^+ level. But if we introduce renormalized transmission coefficients into the calculations, choosing them in such a way that at a neutron energy below 100 keV they would correspond to the experimental strength functions (s_o for even and s_1 for odd partial waves) and at 2-3 MeV would smoothly change to the transmission coefficients of the unified optical model, the description of the near-threshold sector of the excitation functions improves considerably (see Fig. 21). A similar effect can be achieved by the choice of the optical potential parameters V_v and W_s [74]. In this case, the energy dependence of the optical model parameters in the region of low energies ($E_n \lesssim 3$ MeV) will differ substantially from that observed at higher energies [77]. It should be pointed out that "renormalization" of the transmission coefficients to the resonance values of the strength functions is generally necessary for a consistent description of the total neutron cross-sections and the neutron radiative capture cross-sections for low energies $E_n \lesssim 1$ MeV [63].

We encounter an effect of the same nature, although it occurs in a somewhat different manner, in the analysis of near-threshold sectors of the neutron excitation functions for the first levels of heavier nuclei [78]. Figure 22 shows the observed neutron inelastic scattering cross-sections at 300 keV above the threshold for the 2^+ level and the results of theoretical description of these cross-sections. The transmission coefficients used in the theoretical calculations in the strongly-coupled channel model with the optical potential parameters V_v = 53-54 MeV and W_s = 2-3 MeV, which optimally describe the neutron strength functions for the s- and p-resonances. With such a choice of parameters the inelastic scattering cross-sections, too, are reproduced fairly well for most nuclei (see Fig. 22). However, in the case of some Ge, Se and Te isotopes, we observe considerable disagreement between calculations and experimental data. A more detailed analysis of these isotopes showed that agreement with experiment could be achieved by considering the coupling of a fairly large number of inelastic scattering channels and simultaneously reducing the imaginary part of the optical potential W_s to 1 MeV [78]. This leads to a substantial increase in the contribution of direct transitions, which, in the case of particular partial waves (especially p-waves), may even exceed, in the near-threshold region, the partial neutron scattering cross-section for the compound mechanism. The given result indicates that there may be a strong correlation between the neutron widths of p-resonances in some Ge, Se and Te isotopes. It will be of great interest to make a further study of similar correlations in order to improve our ideas about nuclear reaction mechanisms.

Since strength function calculations with the optimum sets of optical potential parameters still reproduce, on the average, the general characteristics of the behaviour of the transmission coefficients reasonably well, it is natural that in the case of many nuclei we do not observe substantial deviations of the experimental excitation functions from the theoretical description obtained with a "unique" optical potential. However, in the case of nuclei exhibiting the above characteristics of the energy dependence of the excitation functions for the first levels, requiring for their explanation a substantial change of the potential parameters in the low-energy region, we should expect similar effects also in the excitation functions for all subsequent levels, including the region of unresolved levels. Experimental study of these effects could provide information on the differences between the optical potential for the ground and excited states of nuclei. Highly interesting results along these lines were obtained by the authors of Ref. [79], who have shown that it is possible to obtain the energy dependence of the cross-section of neutron absorption by the highly-excited nucleus ($U \approx$ 8-12 MeV) from an analysis of the low-energy sector of the neutron spectra of the (p,np') reaction for the Ni, Zr and Sn nuclei. The cross-sections found indicate an appreciable difference in neutron absorption in the case of the excited and non-excited nuclei; however, the accumulated data are still too few to draw unambiguous conclusions concerning the change in the optical potential in highly-excited nuclei.

Some indications of the expected differences in the transmission coefficients for the ground and first excited states of nuclei can be obtained from the calculations of neutron strength functions in the strongly-coupled channel model [11,12]. Within the framework of this model we can take as the entrance channel any of the explicitly open scattering channels and investigate the resulting changes in the strength functions or transmission coefficients. Table 6 gives, as an example, the calculated values of the transmission coefficients for the s- and p-neutrons in the case of the ground and first excited states of the ^{56}Fe and ^{92}Zr nuclei at 0.1 and 1.0 MeV [12]. At low neutron energies (below 0.1 MeV) the differences in the transmission coefficients are very considerable but decrease appreciably with increase in incident-neutron energy.

These calculations suggest that the conventional procedure for identifying the transmission coefficients for the ground and excited states of nuclei can in a certain way distort the results of analysis of the low-energy sectors of the level excitation functions and that these distortions can be very substantial in the region of maxima of the corresponding strength functions. Therefore, although the inclusion of the effects discussed here in the description of neutron cross-sections results in complicating the analysis, this is evidently unavoidable when we consider experimental data which are undergoing constant refinement.

CONCLUSION

The main results of the above studies on neutron scattering for the low-lying levels of light and medium nuclei can be briefly summarized as follows:

1. In the analysis of neutron differential elastic scattering cross-sections a large part of unjustified fluctuations in the optical potential parameters can be eliminated by going over from the single-channel optical model to the coupled-channel unified model. Within the framework of the unified optical model the characteristics of the energy and the isotopic changes in the potential depth can be investigated far more effectively, for example, the existing difference in the energy dependence of the imaginary part of the optical potential at neutron energies up to 15 MeV and in the region of higher energies;

2. Precision measurements of neutron differential inelastic scattering cross-sections for the lowest collective levels of even-even nuclei afford a very effective means of studying the structural differences in the isoscalar and isovector components of nuclear excitations. Such differences have so far been studied only for the lowest quadrupole excitations of near-magical nuclei with a closed proton Z = 50 or neutron N = 50 shell, and it is of considerable interest to study similar effects during the excitation of higher levels;

3. The direct inelastic scattering mechanism makes a substantial contribution to the observed excitation cross-sections for the lowest collective levels of nuclei even at comparatively low neutron energies $E_n \lesssim 3$ MeV. Consideration of direct transitions reduces the integral cross-sections for neutron scattering with compound nucleus formation and, consequently, changes the transmission coefficients for the different partial waves. Analysis of the excitation functions for the 4_1^+ and 0_2^+ levels of the ^{28}Si nucleus demonstrates the important role played by these changes in the consistent description of experimental data. A study of such changes for a wider group of nuclei will help in further improving the methods of theoretical analysis of nuclear reaction cross-sections and also in refining the optical potential parameters used in many practical applications of neutron physics;

4. In the description of the near-threshold sectors of the level excitation functions it is fundamentally important to take into account the individual structural irregularities of changes in the neutron strength functions. At present, the influence of these irregularities has been investigated only for a limited number of lowest levels of even-even nuclei. A broadening of this trend in research may become very fruitful in the investigation of the differences in the optical potential for the ground and excited states of nuclei.

The authors are grateful to I.A. Korzh, G.N. Lovchikova and N.M. Pravdivyj for numerous and fruitful discussions of the problems considered in this paper.

REFERENCES

1. BLATT, J.M., WEISSKOPF, V.F., Theoretical Nuclear Physics, Ed. John Wiley and Sons N.Y. (1952).

2. LANE, A., THOMAS, R., The Theory of Nuclear Reactions at Low Energies (Russian translation, 1960).

3. **Austern N.** Direct Nuclear Reaction Theories. N. Y., Wiley Interscience, 1970.

4. **Lynn J. R.** Theory of Neutron Resonance Reactions. Oxford, Clarendon Press, 1968.

5. HODGSON, P.E., The Optical Model of Elastic Scattering, Clarendon Press, Oxford (1960).

6. MARCHUK, G.I., KOLESOV, V.E., The Use of Numerical Methods in Neutron Cross-Section Calculations, Atomizdat, Moscow (1966).

7. **Prince A.** Nuclear Theory in Neutron Nuclear Data Evaluation. V. 1. Vienna. IAEA-190, 1976, p. 31.

8. BOHR, O., MOTTELSON, B., The Structure of the Atomic Nucleus, Vol. 2 (Russian translation, 1977).

9. **Tamura T.**— Rev. Mod. Phys., 1965, v. 37, p. 679.

10. IGNATYUK, A.V., LUNEV, V.P., SHORIN, V.S., Problem of Atomic Science and Technology, Ser. Nuclear Constants 13 (1974) 59.

11. **Dunford Ch., Fenech H., Reinolds Z.**— Phys. Rev., 1969, v. 177, p. 1395.

12. IGNATYUK, A.V., LUNEV, V.P., in: Neutron Physics, part 1, TSNIIAI, Moscow (1980) 77.

13. **Moldauer P.**— Rev. Mod. Phys., 1964, v. 36, p. 1079.
14. **Hoffmann N. M. e.a.**— Ann. Phys., 1975, v. 90, p. 403.
15. **Moldauer P.** Nuclear Theory for Applications. Trieste, IAEA-SMR-43, 1980, p. 165.
16. **Tepel J., Hoffmann H., Weidenmüller H.**— Phys. Lett. B, 1974, v. 49, p. 1.
17. **Becchetti F. D., Greenlees G. W.**— Phys. Rev., 1969, v. 182, p. 1190.
18. **Holmqvist B., Wiedling T.**— Nucl. Phys. A, 1972, v. 188, p. 24.
19. **Holmqvist B., Wiedling T.**— J. Nucl. Energy, 1973, v. 27, p. 543.

20. PASECHNIK, M.V., KORZH, I.A., KASHUBA, I.E., in: Neutron Physics, part 1, Naukova Dumka, Kiev (1972) 253.

21. **Bainum D. E. e.a.**— Nucl. Phys. A, 1978, v. 311, p. 492; **Rapaport J. e.a.**— Nucl. Phys. A, 1980, v. 341, p. 56.
22. **Tanaka S.**— In: Proc. EANDC Topical Discussion on «Critique of Nuclear Models and their Validity in Evaluation of Nuclear Data». JAERI-5984, 1975, p. 212.
23. **Tanaka S. e.a.**— In: Nuclear Data for Reactors. V. 2. Vienna, IAEA, 1970, p. 317.
24. **Rober J., Brandenberger J.**— Phys. Rev., 1967, v. 163, p. 1077.
25. **Delaroche J. P., Lagrange Ch., Salvy J.**— In: Nuclear Theory in Neutron Nuclear Data Evaluation. V. I. Vienna, IAEA-190, 1976, p. 251.
26. **Ferguson A. e.a.**— In: Proc. Intern. Conf. on Interaction of Neutrons with Nuclei. Lowell, 1976, p. 204.
27. **Haouat G.**— In: Neutron Induced Reactions (Proc. of Second Intern. Symp. in Smolenice). Bratislava, VEDA, 1980, p. 333.
28. **Stelson P. H., Grodzins L.**— Nucl. Data A, 1965, v. I, p. 21.
29. **Veje C. J.**— Mat. fys. medd. Kgl. danske vid. selskab, 1966, v. 35, № 1.
30. **Brown V. R., Madsen V. A.**— Phys. Rev. C, 1975, v. 11, p. 1298; **Madsen V. A., Brown V. R., Anderson J. D.**— Phys. Rev. C, 1975, v. 12, p. 1205.
31. **Finlay R. W. e.a.**— Nucl. Phys. A, 1980, v. 338, p. 45.

32. BLOKHIN, A.I., IGNATYUK, A.V., LUNEV, V.P., in: Neutron Physics, part 1, TSNIIAI, Moscow (1980) 89.

33. **Lachkar J. e.a.**— Phys. Rev. C, 1976, v. 14, p. 933.
34. **Matoba M. e.a.**— Nucl. Phys. A, 1979, v. 325, p. 389.
35. **Compte L.e.a.**— Nucl. Phys. A, 1977, v. 284, p. 123.

36. STRIZHAK, V.I., et al., Fast Neutron Physics, Chapter 2, Atomizdat, Moscow (1977).

37. **Clarke R. L., Cross W. G.**— Nucl. Phys., 1964, v. 53, p. 177; **Martin P. W. e.a.**— Nucl. Phys., 1965, v. 61, p. 524; **Stelson P. H. e.a.**— Nucl. Phys., 1965, v. 68, p. 97.
38. **Drake M. K. e.a.**— Nucl. Phys. A, 1969, v. 128, p. 209.
39. **Kinney W. E., Perey F. G.**— ORNL-4517 and 4539, 1970.
40. **Brandenberger J. D., Mittler A., Ellistrem M. T. Mc.**— Nucl. Phys. A, 1972, v. 196, p. 65.
41. **Obst A. W., Weil J. L.**— Phys. Rev. C, 1973, v. 7, p. 1076.
42. **Velkley D. E. e.a.**— Phys. Rev. C, 1974, v. 9, p. 2181.
43. **Pilz W. e.a.**— In: Neutron Induced Reactions. Bratislava, VEDA, 1980, p. 127;— In: Proc. IX Intern. Symp. on Interaction of Fast Neutrons with Nuclei. Dresden, ZfK-410, 1980, p. 57.
44. **Schmidt D., Seeliger D., Streil T.**— In: Proc. X Intern. Symp. on Interaction of Fast Neutrons with Nuclei. Dresden, ZfK-459, 1981, p. 164; Streil T.- Dr. Thesis, TU Dresden, 1981.
45. **Aleonard M. M. e.a.**— Nucl. Phys. A, 1970, v. 146, p. 90; **Huang F., Daniels D. K. Mc.**— Phys. Rev. C, 1970, v. 2, p. 1342.
46. **Mermaz M. C. e.a.**— Phys. Rev., 1969, v. 187, p. 1466; **Rebel H. e.a.**— Nucl. Phys. A, 1972, v. 182, p. 145.

47. Blair A. G. e.a.— Phys. Rev. C, 1970, v. 1, p. 444.
48. Swinarski R. De. e.a.— Nucl. Phys. A, 1976, v. 261, p. 111.
49. Leo R. De. e.a.— Phys. Rev. C, 1979, v. 19, p. 646.
50. Petitt G. A. e.a.— Nucl. Phys., 1966, v. 79, p. 231.
51. Knitter W. E., Coppola M.— Z. Phys., 1967, Bd 207, S. 56.
52. Schweitzer Th. e.a.— Kernenergie, 1977, Bd 6, S. 174.

53. KORZH, I.A., MISHCHENKO, V.A., SANZHUR, I.E. Ukr. Fiz. Zh. 25 (1980) 109.

54. Cierjacks S. e.a.— KfK-1000, Karlsruhe, 1968.
55. Schouky I. KfK-2503, Karlsruhe, 1977.
56. Hermsdorf D., Neumann L.— In: Proc. IX Intern. Symp. on Interaction of Fast Neutrons with Nuclei. Dresden, ZfK-410, 1980, p. 147.
57. Adel-Fawzy M. e.a.— In: Proc. IX Intern. Symp. on Interaction of Fast Neutrons with Nuclei. Dresden, ZfK-410, 1980, p. 60.
58. Förtsch H.— Dr. Thesis, TU Dresden, 1981.
59. Schweitzer T., Seeliger D., Unholzer S.— In: Proc. VIII Intern. Symp. on Interaction of Fast Neutrons with Nuclei. Dresden, ZfK-382, 1979, p. 125.

60. KORZH, I.A., et al., Yad. Fiz. 35 (1982) 1097.

61. Van Patter D. M. e.a.— Phys. Rev., 1962, v. 128, p. 1246.

62. BRODER, D.L., et al., At. Ehnerg. 18 (1964) 645.

63. Kinney W. E., Perey F. G.— ORNL-4806, 1974.
64. Karatzas P. T. e.a.— Nucl. Sci. Engng., 1978, v. 67, p. 34.

65. BYCHKOV, V.M., et al., Problems of Atomic Science and Technology, Ser. Nuclear Constants 19 (1975) 110.

66. Smith A. e.a.— Nucl. Sci. Engng., 1979, v. 72, p. 293.

67. KORZH, I.A., et al., At. Ehnerg. 50 (1981) 398.

68. Mohamed A. H. e.a.— In: Proc. IX Intern. Symp. on Interaction of Fast Neutrons with Nuclei. Dresden, ZfK-410, 1980, p. 34.
69. Tsukada K.— Nucl. Phys. A, 1969, v. 125, p. 641.

70. KORZH, I.A., Ukr. Fiz. Zh. 22 (1977) 87.

71. Smith A., Guenther P.— Nucl. Sci. Engng., 1980, v. 73, p. 186.
72. Mughabghab S. F., Divadeenam M., Holden N. E. Neutron Cross Sections. V. I. N. Y.— L., Academic Press, 1981.
73. Müller K. N., Rohr G.— Nucl. Phys. A, 1971, v. 164, p. 97.
74. Newstead C. M., Delaroche J., Canvin B.— In: Statistical Properties of Nuclei. N.Y., Plenum Press, 1972, p. 367.
75. Feshbach H., Kerman A. K., Lemmer R. H.— Ann. Phys., 1967, v. 41, p. 230.

76. ADAMCHUK, Yu.V., SIROTKIN, V.K., Yad. Fiz. 26 (1977) 495.

77. Benzi V., Fabbri F., Reffo G.— In: Proc. EANDC Topical Discussion on «Critique of Nuclear Models and Their Validity in Evaluation of Nuclear Data». JAERI-5984, 1975, p. 83.

78. EFROSININ, V.P., MUSAELYAN, R.M., POPOV, V.I., Yad. Fiz. 29 (1979) 631; KONOBEEVSKIJ, E.S., POPOV, V.I., Report P-0155, Nuclear Research Institute, USSR Academy of Sciences, Moscow (1980).

79. Rao G. R. e.a.— Phys. Rev. C, 1973, v. 7, p. 733.

Table 1 Dynamic deformation quadrupole parameters obtained during excitation of the lowest 2^+ levels of nuclei with a filled neutron N = 50 or proton Z = 50 shell*/ [27]

Deformation parameters		Nuclei with $N=50$			Nuclei with $Z=50$				
		^{88}Sr	^{90}Zr	^{92}Mo	^{116}Sn	^{118}Sn	^{120}Sn	^{122}Sn	^{124}Sn
Experiment [21, 31]	$\beta_2^{(n)}$	0,133 (7)	0,085 (8)	0,099 (5)	0,120 (10)	0,109 (7)	0,106 (5)	0,100 (6)	0,092 (6)
	$\beta_2^{(p)}$	0,11	0,070 (5)	0,080 (6)	0,133	0,134 (10)	0,119 (10)	0,112 (7)	0,108 (7)
	$\beta_2^{(n)}/\beta_2^{(p)}$	1,2	1,2	1,3	0,90	0,81	0,90	0,90	0,85
	$\beta_2^{(\gamma)}$	0,14 (2)	0,094 (5)	0,116 (8)	0,118 (7)	0,108 (2)	0,106 (2)	0,102 (2)	0,096 (2)
Theory [31]		$\beta_2^{(\gamma)} > \beta_2^{(n)} > \beta_2^{(p)}$			$\beta_2^{(\gamma)} < \beta_2^{(n)} < \beta_2^{(p)}$				
	$\beta_2^{(n)}/\beta_2^{(p)}$	1,35	1,33	1,31	0,88	0,89	0,90	0,90	0,91
	$\beta_2^{(\gamma)}$	0,15	0,093	0,109	0,105	0,093	0,099	0,094	0,084

*/ The figures in brackets determine the error in the last figures of the experimental values for the deformation parameters.

Table 2 Quadrupole deformation parameters for the first 2^+ levels of Se isotopes

Isotope	$\beta_2^{(n)}$ [33]	$\beta_2^{(p)}$ [34]	$\beta_2^{(\gamma)}$ [35]
^{76}Se	0,28 (1)	0,278 (7)	0,310 (2)
^{78}Se	0,27 (1)	0,243 (6)	0,268 (3)
^{80}Se	0,25 (1)	0,210 (5)	0,232 (2)
^{82}Se	0,22 (1)	0,159 (4)	0,192 (2)

Table 3 Neutron inelastic scattering cross-sections at 3.4 MeV for the first levels of light nuclei

Target nucleus	Level Energy, MeV	J^π	σ_{exp}, mb	$\sigma_{calc}^{H.F.M.}/\sigma_{exp}$, %
^{23}Na	0,439	$5/2^+$	443±94	55
^{24}Mg	1,369	2^+	511±93	91
^{27}Al	0,842	$1/2^+$	130±23	59
	1,013	$3/2^+$	170±30	88
^{28}Si	1,779	2^+	588±177	79
^{31}P	1,270	$3/2^+$	429±88	55

Table 4 Neutron inelastic scattering cross-sections at 3.4 MeV for the low-lying levels of nuclei of the iron group

Target nucleus	Level energy, MeV	I^{π}	σ_{exp}, mb	$\sigma_{calc}^{H.F.M.}/\sigma_{exp}$, %	$\sigma_{calc}^{direct}/\sigma_{exp}$, %
^{51}V ($I_0^{\pi}=7/2^-$)	0,319	$5/2^-$	287±32	80	4,6
	0,928	$3/2^-$	134±15	86	6,5
	1,609	$11/2^-$	265±29	90	7,5
	1,813	$9/2^-$	308±34	76	5,2
^{55}Mn ($I_0^{\pi}=5/2^-$)	0,983	$9/2^-$	164±26	86	15,7
	1,289	$11/2^-$	102±16	88	29,2
	1,527	$3/2^-$	90±15	116	9,3
	1,884	$7/2^-$	81±19	112	—
^{56}Fe	0,845	2^+	643±114	72	12,4
^{59}Co ($I_0^{\pi}=7/2^-$)	1,099	$3/2^-$			
	1,190	$9/2^-$	255±41	104	10,8
	1,291	$3/2^-$			
	1,434	$1/2^-$			
	1,460	$11/2^-$	273±44	91	11,2
	1,481	$5/2^-$			
	1,744	$7/2^-$	112±12	96	17,2

Table 5 Neutron strength functions for even-even nuclei of the iron group (in units of 10^{-4})

Target nucleus	Spherical optical model		Strongly-coupled channel model		Experiment [72]	
	s_0	s_1	s_0	s_1	s_0	s_1
^{50}Cr	3,64	1,25	4,90	1,34	3,6±0,8	0,33±0,12
^{52}Cr	5,32	0,96	4,82	1,15	2,5±0,9	0,52±0,12
^{54}Cr	—	—	3,05	1,17	2,8±1,0	—
^{54}Fe	—	—	5,18	0,83	8,7±2,4	0,58±0,11
^{56}Fe	4,62	0,80	3,05	0,93	2,6±0.6	0,45±0,05
^{58}Fe	—	—	2,64	0,88	3,6±1,2	0,6±0,2
^{58}Ni	—	—	3,01	0,81	2,8±0,6	0,5±0,1
^{60}Ni	3,90	0,74	2,53	0,81	2,7±0,6	0,3±0,1
^{62}Ni	—	—	2,45	0,80	2,8±0,7	0,3±0,1
^{64}Ni	—	—	2,43	0,79	2,9±0,8	0,6±0,2

Table 6 Transmission coefficient T_{lj} for the ground and first excited states of nuclei

Target nucleus	E_n, MeV	State	$T_{0\,1/2}$	$T_{1\,1/2}$	$T_{1\,3/2}$
^{56}Fe $\beta_2=0,24$	0,1	Ground	0,526	0,0135	0,0100
		Excited	0,742	0,0086	0,0074
	1,0	Ground	0,832	0,158	0,140
		Excited	0,735	0,113	0,110
^{92}Zr $\beta_2=0,13$	0,1	Ground	0,089	0,143	0,282
		Excited	0,068	0,074	0,164
	1,0	Ground	0,215	0,946	0,964
		Excited	0,180	0,758	0,873

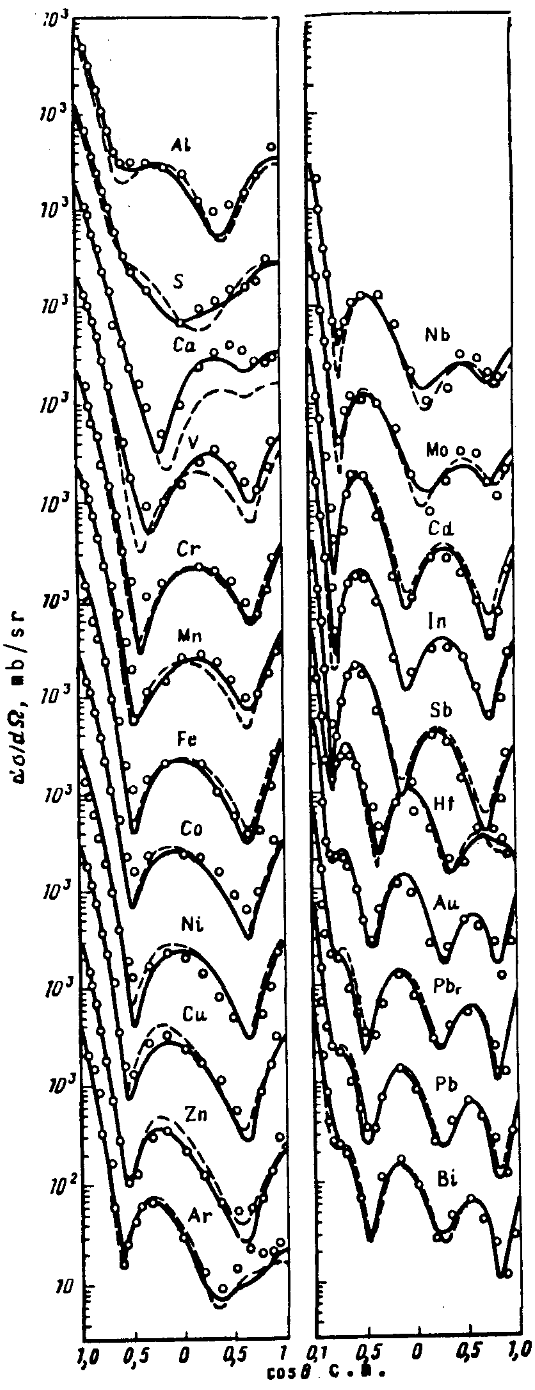

Fig. 1 Differential cross-sections for elastically scattered neutrons at 8.05 MeV:
o - experimental data; ——— - theoretical calculations with individually chosen parameters;
- - - - - with parameter set (19).

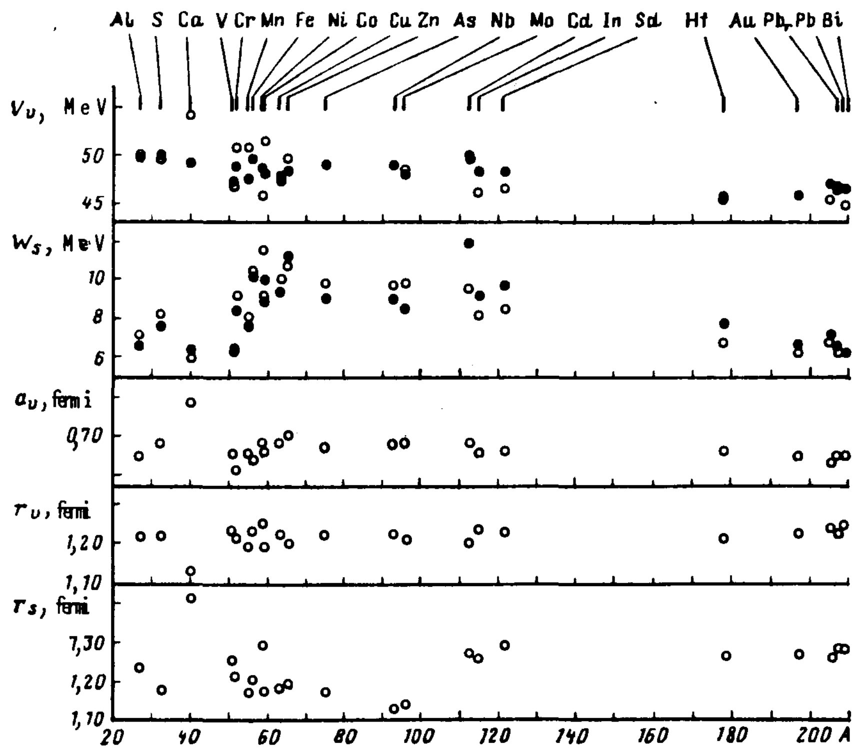

Fig. 2 Optical potential parameters obtained from the description of neutron elastic scattering (see Fig. 1): o – with the adjustment of all potential parameters; • – with fixed geometrical parameters (19).

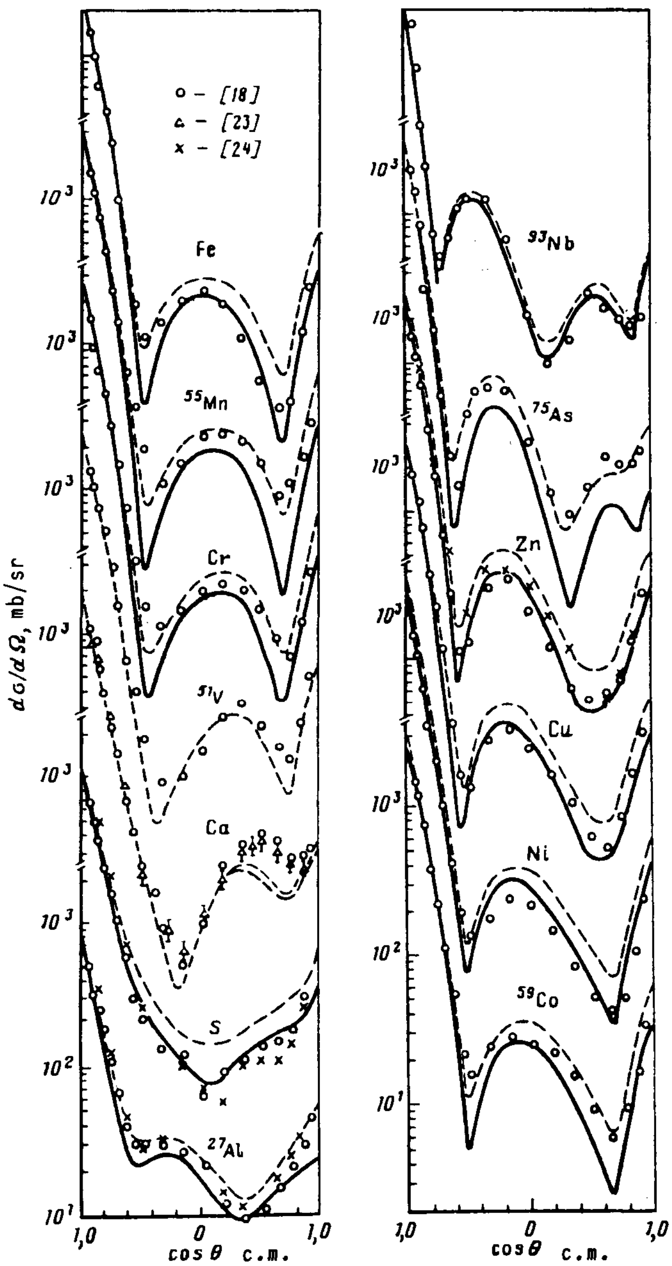

Fig. 3 Theoretical description of the differential elastic scattering cross-sections for 8.05-MeV neutrons in the strongly-coupled channel model (solid lines) and in the spherical optical model (dashed lines) with the parameter set (23)

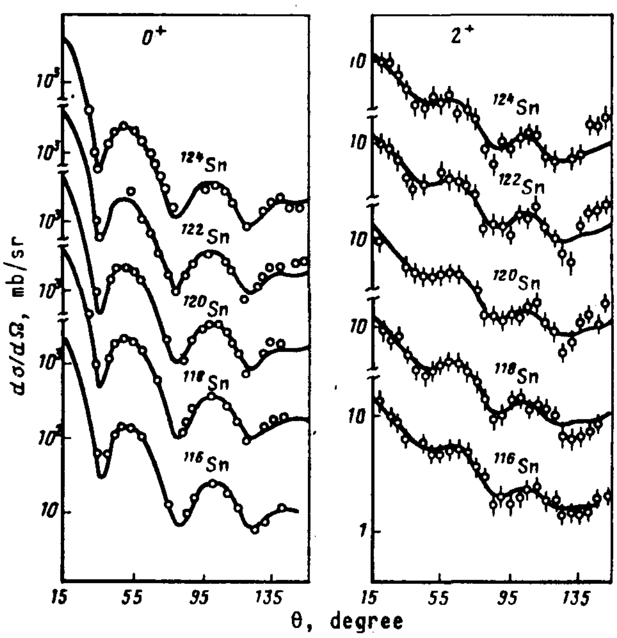

Fig. 4 Experimental data and theoretical description of the elastic and inelastic scattering cross-sections for 11-MeV neutrons in tin

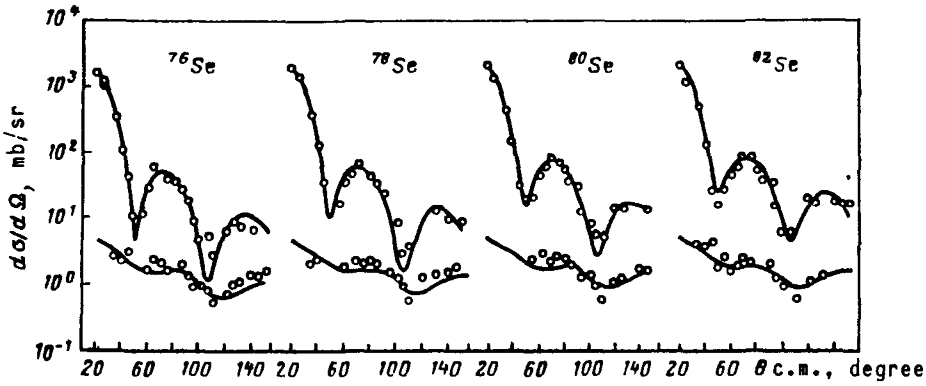

Fig. 5 Same as Fig. 4 for selenium isotopes at 8 MeV neutron energy

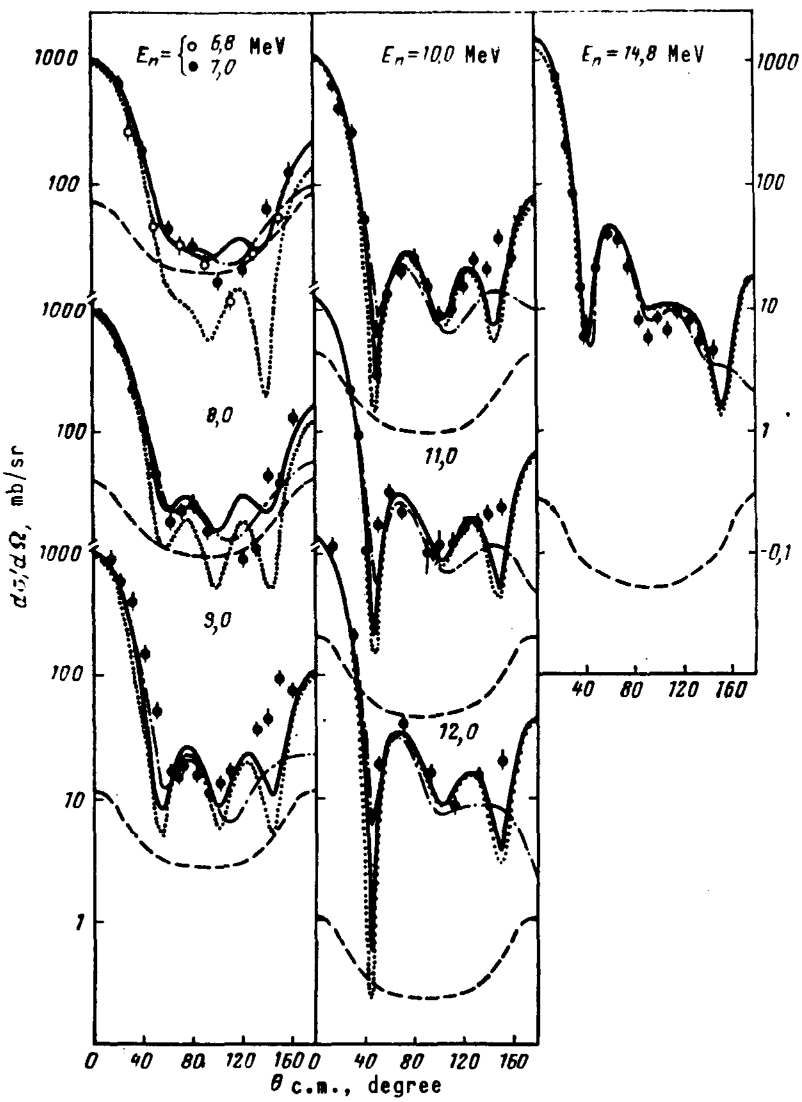

Fig. 6 Neutron differential elastic scattering cross-sections for the ^{28}Si isotope (points) and the various components of their theoretical description: - - - - cross-section for scattering with compound nucleus formation; dotted line - potential scattering cross-section in the strongly-coupled channel model; solid line - sum of the cross-sections for the two scattering mechanisms in the strongly coupled channel model; dot-dash line - same cross-sections in the spherical optical model

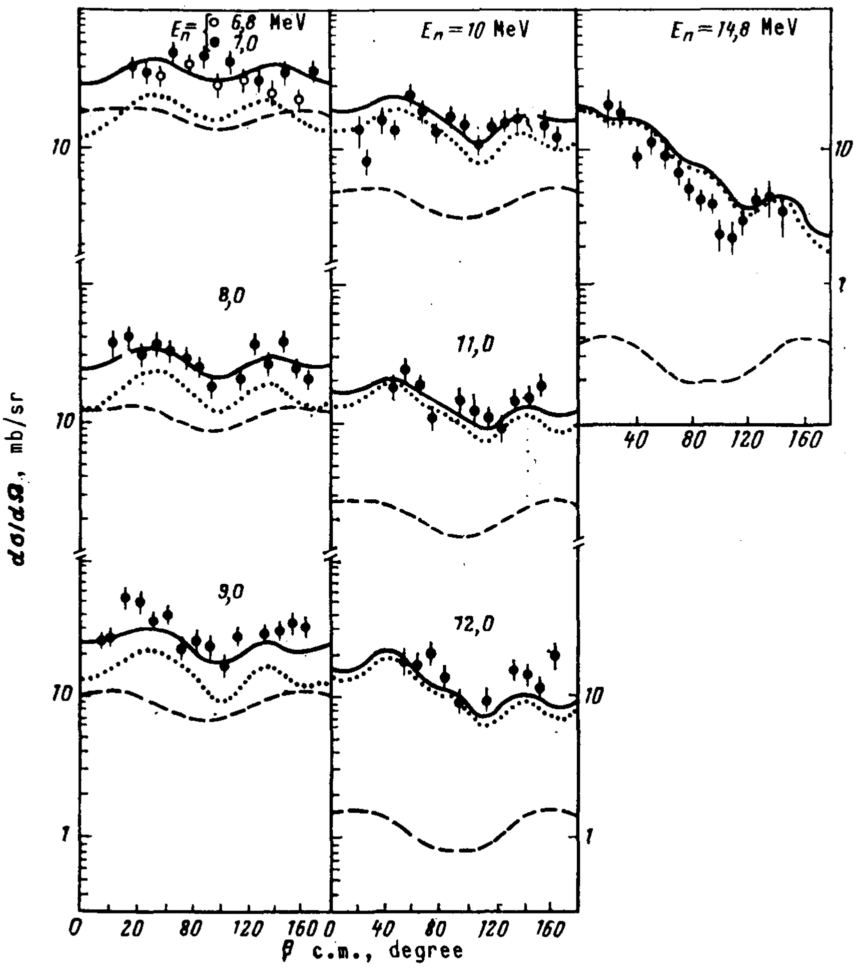

Fig. 7 Neutron differential inelastic scattering cross-sections for the first 2^+ level of the ^{28}Si nucleus: the notations for the theoretical curves are the same as in Fig. 6

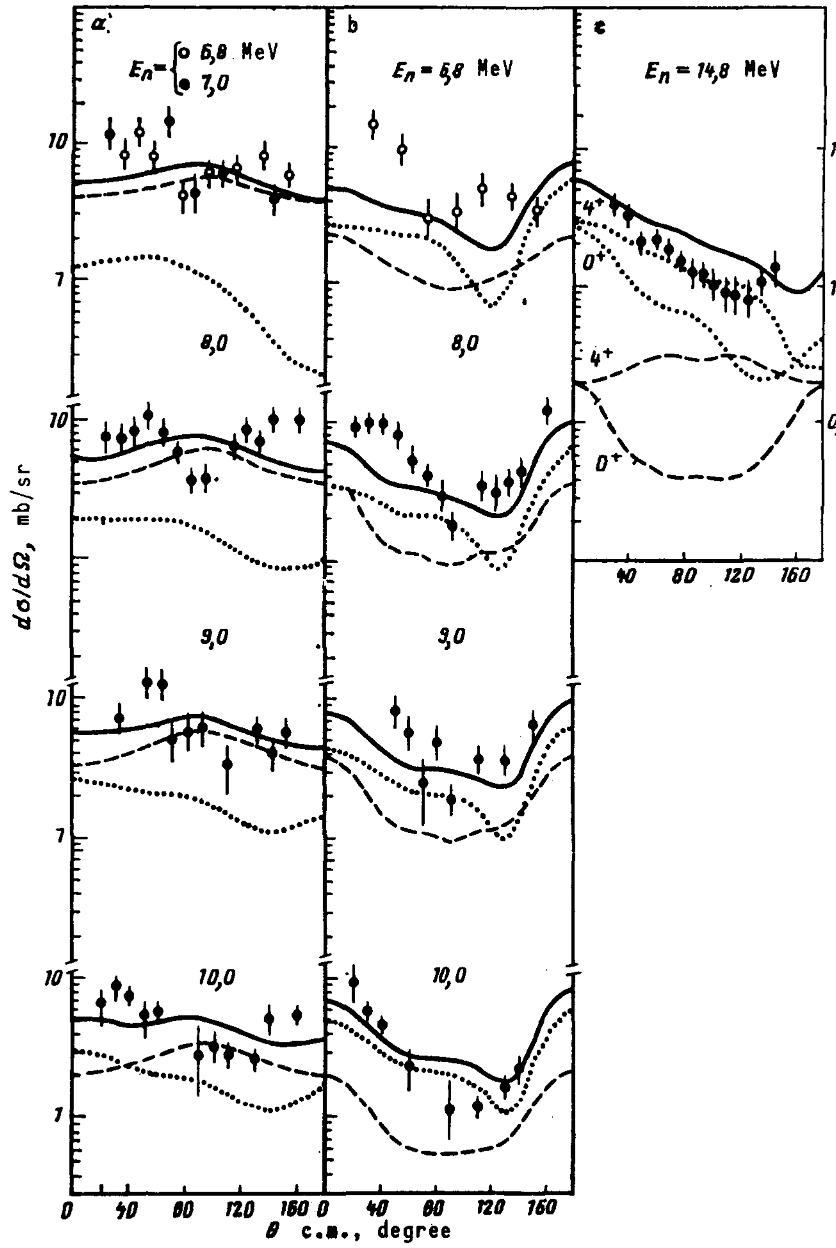

Fig. 8 Neutron differential inelastic scattering cross-sections for levels 4_1^+ (a), and 0_2^+ (b) of the ^{28}Si nucleus. In the case of 14.8-MeV neutrons (c), the experimental points and the solid theoretical curve describe the sum of the scattering cross-sections for the two levels (the notations for the remaining curves are the same as in Fig. 6)

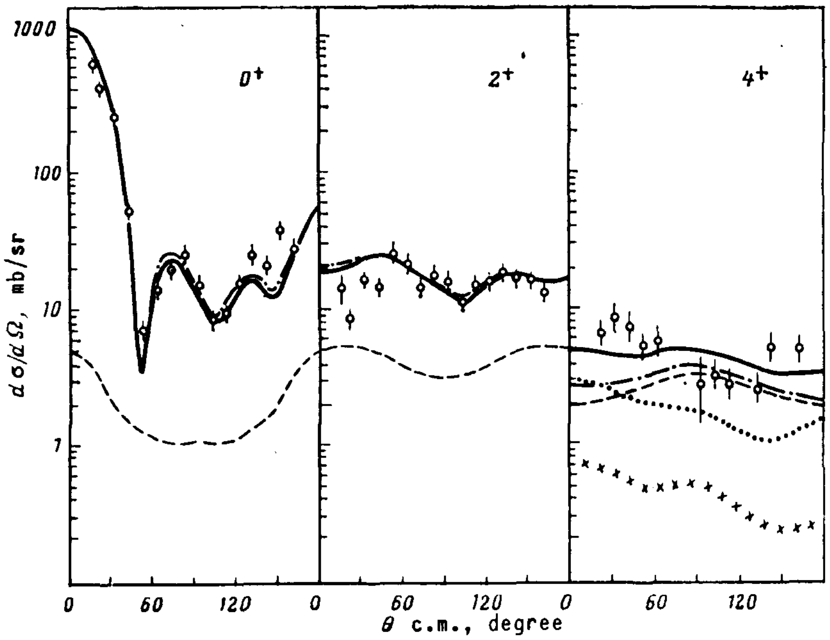

Fig.9 Calculations of elastic and inelastic scattering cross-sections for 10-MeV neutrons based on different assumptions about equilibrium deformation of the ^{28}Si nucleus: solid curve - $\beta_2 = 0.48$, $\beta_4 = -0.30$; dot-dash curve - $\beta_2 = -0.48$, $\beta_4 = 0.10$. For the 4^+ level the cross-sections for direct transitions corresponding to the two assumptions are also shown (dotted and x x x lines)

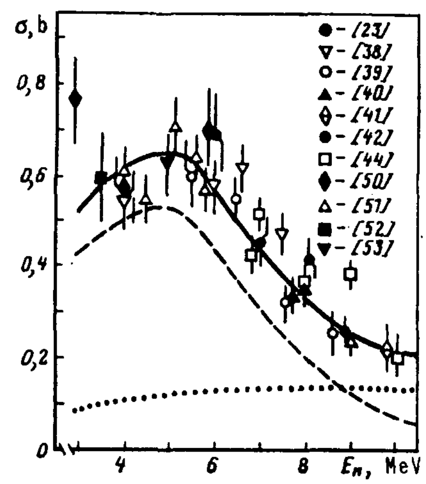

Fig. 10 Neutron integral inelastic scattering cross-sections for the 2^+ level of the ^{28}Si nucleus: dotted curve - direct inelastic scattering cross-section; dashed curve - scattering with compound nucleus formation; solid curve - sum of the cross-sections for the two scattering mechanisms

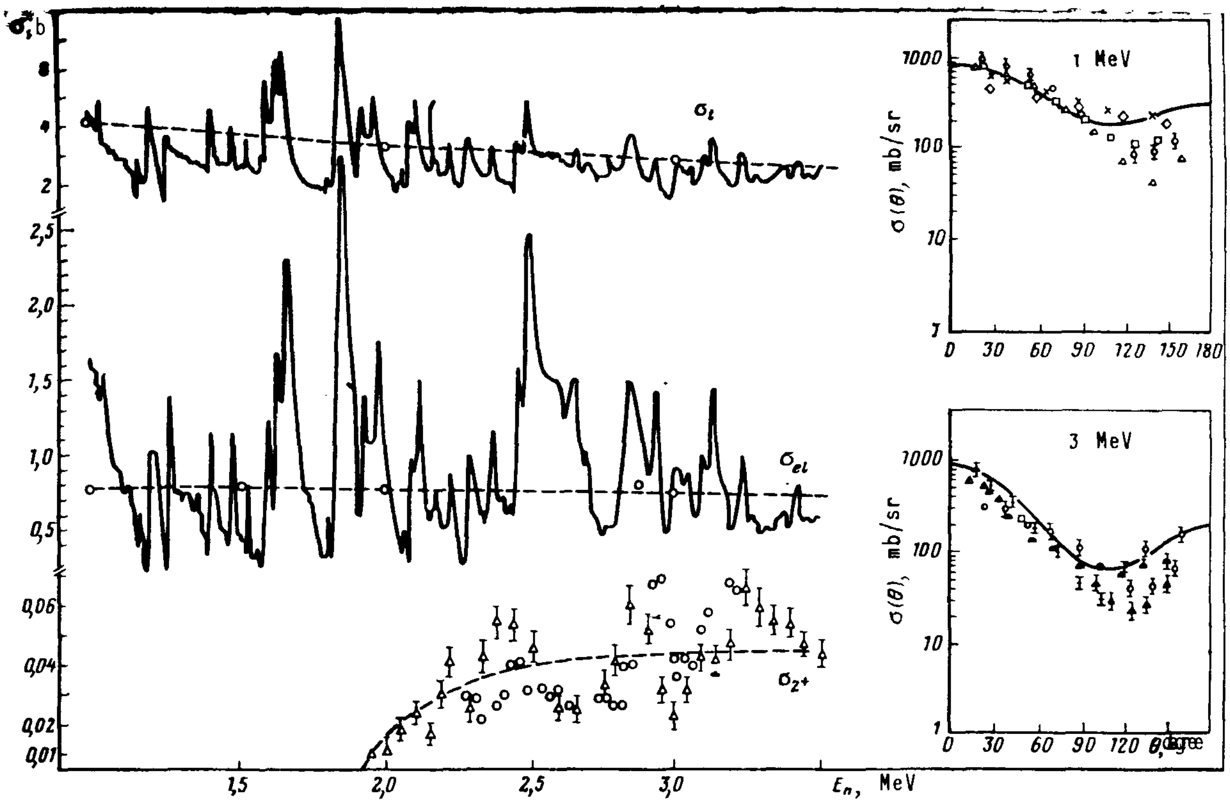

Fig. 11 Dependence of the total cross-section σ_t, elastic scattering cross-section $\sigma_{el}(\theta = 20^o)$ and inelastic scattering cross-section for the first level σ_{2+} ($\theta = 60^o$) of the ^{28}Si nucleus on neutron energy:

solid lines - cross-sections measured in experiements with high energy resolution [54, 55]; dashed lines - description of the average cross-sections within the framework of the optical model; the inserts contain the description of the angular distributionsof elastically scattered neutrons, the experimental points being the compilation of measurements with different energy resolutions [56]

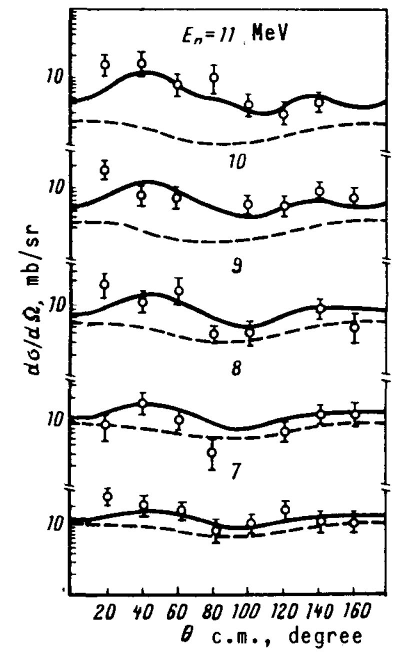

Fig. 12 Neutron differential inelastic scattering cross-sections for the first 2^+ level of the ^{32}S nucleus (the notation for the theoretical curves is similar to that in Fig. 6)

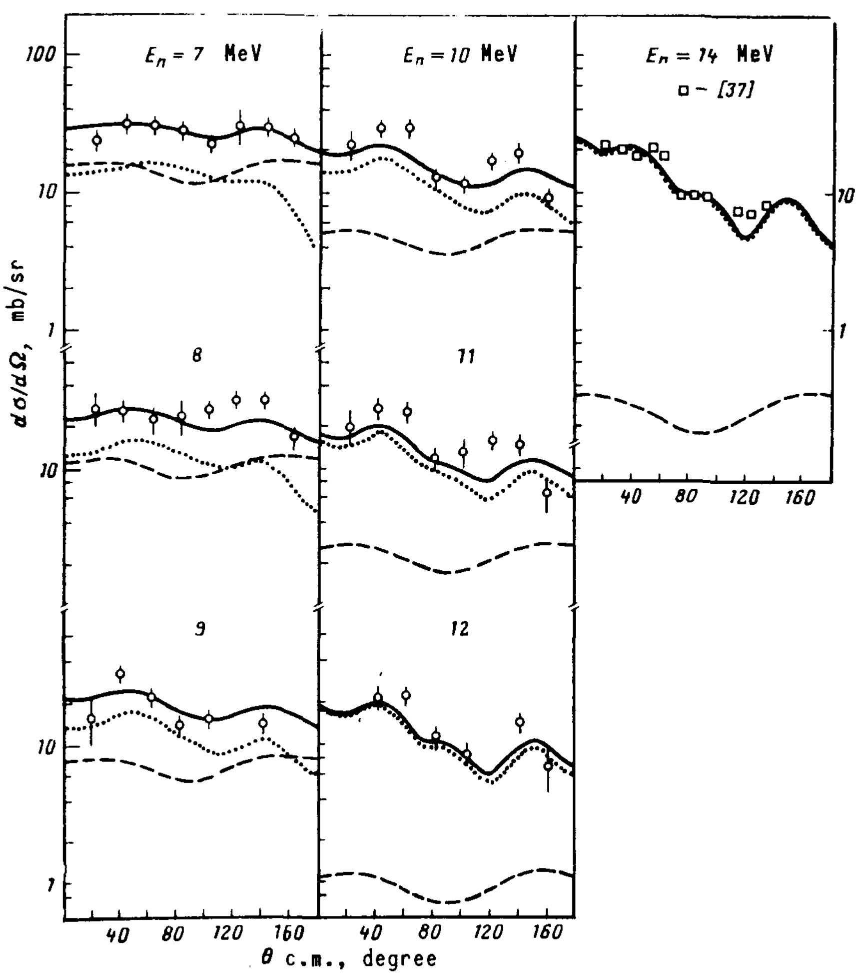

Fig. 13 Same as Fig. 12 for the ^{24}Mg nucleus

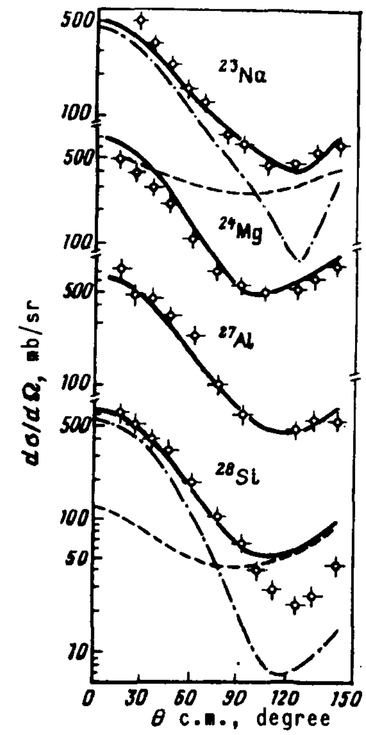

Fig. 14 Differential elastic scattering cross-sections for 3.4-MeV neutrons: dashed line - for cross-section scattering with compound nucleus formation; dot-dash line - direct potential scattering in the strongly-coupled channel model; solid line - the sum of the two scattering mechanisms

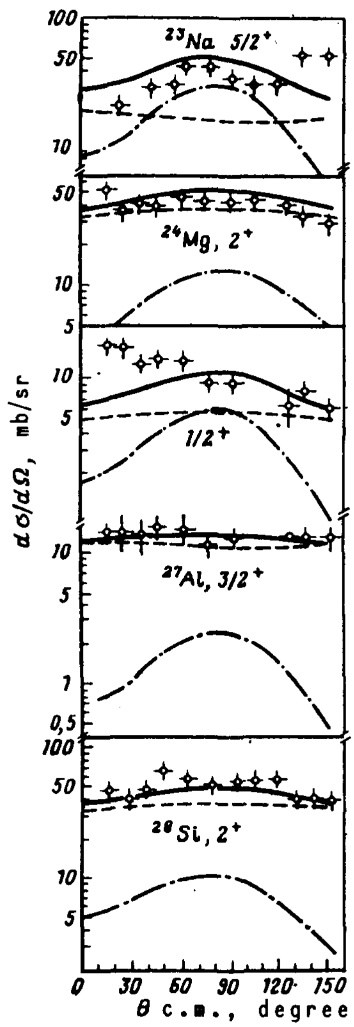

Fig. 15 Same as Fig. 14 for inelastic scattering at the lowest levels (the notations are the same as in Fig. 14)

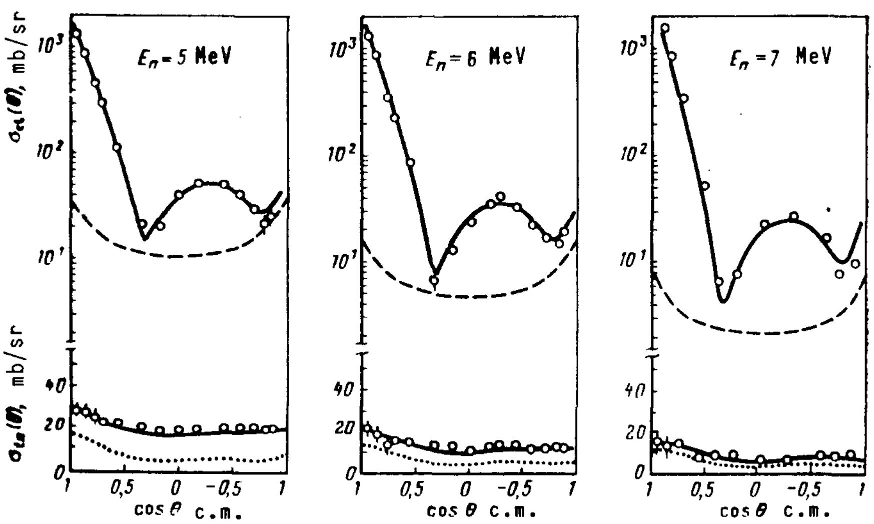

Fig. 16 Neutron differential elastic and inelastic scattering cross-sections for the 2_1^+ level (Q = -1.435 MeV) of the ^{52}Cr nucleus [60] (the notations for the theoretical curves are the same as in Fig. 6)

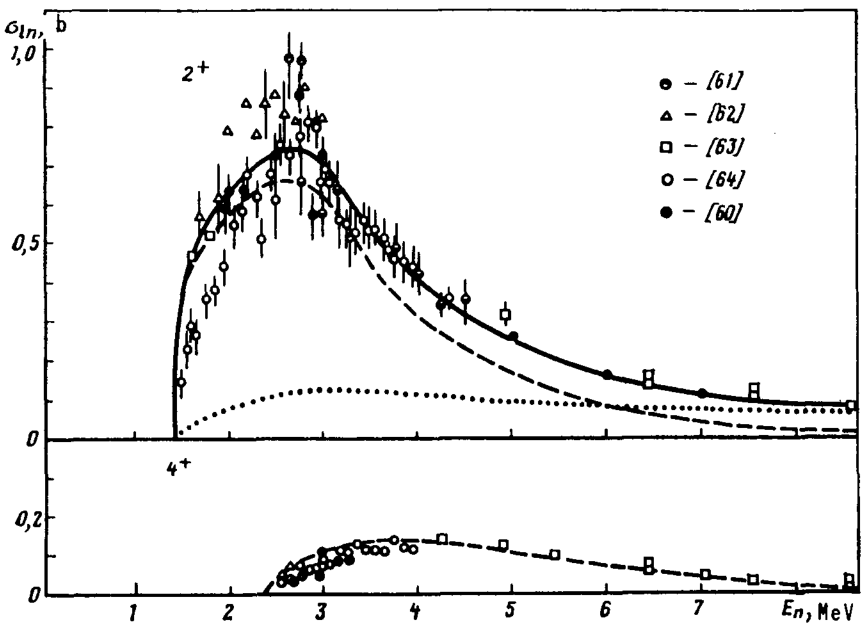

Fig. 17 Neutron integral inelastic scattering cross-section for levels 2_1^+ (Q = -1.435 MeV) and 4_1^+ (Q = -2.370 MeV) of the ^{52}Cr nucleus (the notations for theoretical curves are the same as in Fig. 10)

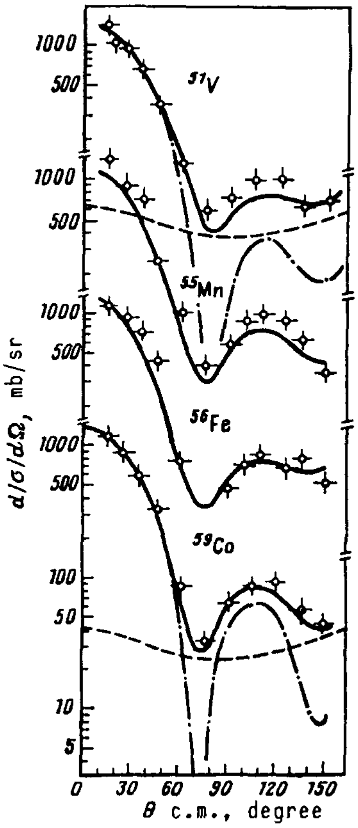

Fig. 18 Neutron differential elastic scattering cross-section at 3.4 MeV for nuclei of the iron group (the notations are the same as in Fig. 14)

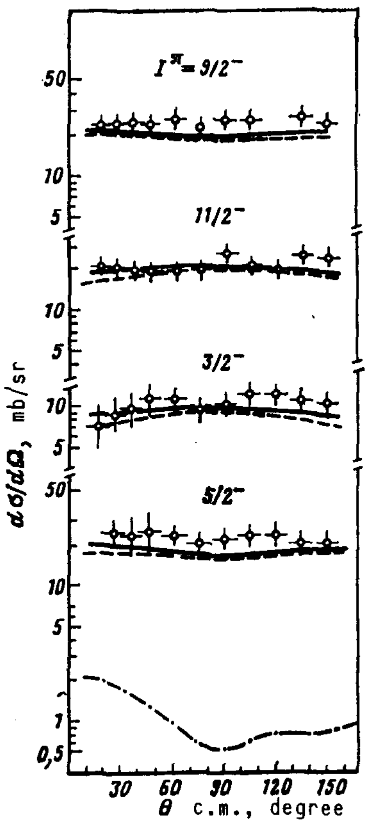

Fig. 19 Neutron differential inelastic scattering cross-sections at 3.4 MeV for the lowest levels of the ^{51}V nucleus

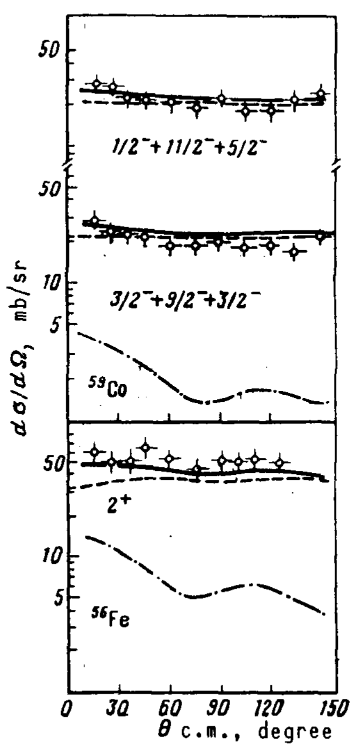

Fig. 20 Same as Fig. 19 for the ^{56}Fe and ^{59}Co nuclei

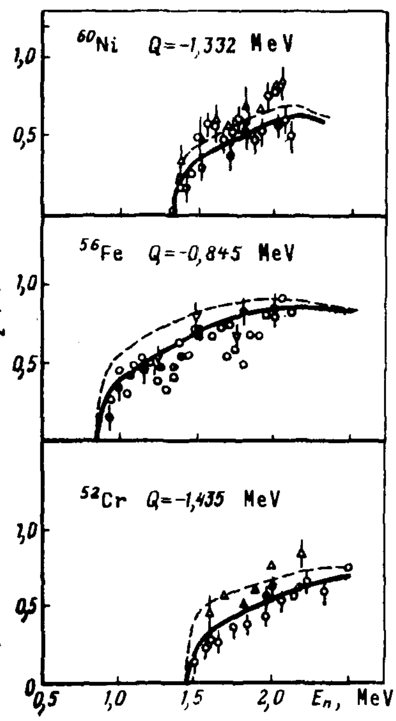

Fig. 21 Description of near-threshold sectors of the excitation functions for the first 2^+ levels of even-even nuclei of the iron group for transmission coefficients of the strongly-coupled channel model (dashed curves) and for coefficients "renormalized" to experimental values of neutron strength functions (solid curves). The experimental points are compilation of the measurements of the various authors [60-64, 66, 70, 71]

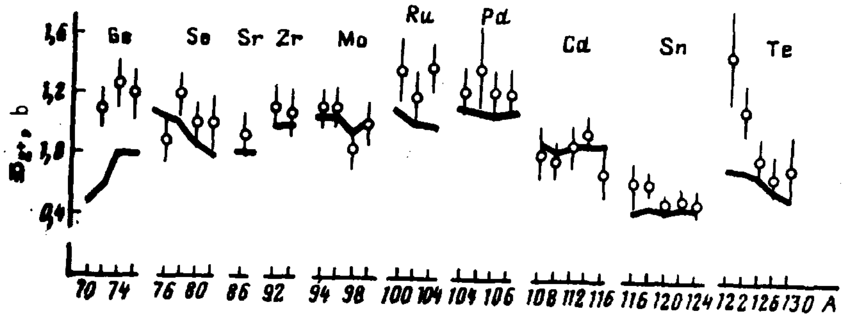

Fig. 22 Neutron inelastic scattering cross-sections at 300 keV above the excitation threshold of the 2_1^+ level (o) and their theoretical description in the strongly-coupled channel model (solid lines)